PHYSICAL REVIEW D **90,** 116007 (2014)

Constructive interference in the spectrum of bremsstrahlung on two amorphous targets

M. V. Bondarenco* and N. F. Shul'ga

NSC Kharkov Institute of Physics and Technology, 1 Academic Street, 61108 Kharkov, Ukraine

(Received 26 July 2014; published 29 December 2014)

We investigate the interference pattern in the spectrum of nondipole bremsstrahlung on two amorphous foils. It contains a suppression at lowest photon energies, an enhancement in the neighboring region, and subsequent evanescent oscillations. The net effect of suppressions and enhancements proves to be zero. The location and the origin of the spectral features is explained. Predictions of the rigorous Molière averaging are compared with those of the Gaussian averaging with Coulomb contributions to the rms multiple scattering angle. Comparison with experimental data and with previous theoretical predictions is included.

DOI: 10.1103/PhysRevD.90.116007 PACS numbers: 41.60.-m, 78.70.-g

I. INTRODUCTION

The suppression of the yield of low-energy bremsstrahlung photons from ultrarelativistic electrons passing through an amorphous scattering medium is commonly known as the LPM effect [1]. More precisely, Landau, Pomeranchuk [2], and Migdal [3] studied it only in the limit of large target thickness. Subsequently, it had been investigated for finite-thickness targets [4–8], and for the opposite limit of a geometrically thin target [4,9], which is of intrinsic interest. The theoretical predictions were accurately tested experimentally within the last two decades [10], and the theoretical and experimental state of the art was reviewed in [11–13].

For many practical applications, as well as from the fundamental point of view, it is also necessary to deal with structured targets. A simple example thereof is a sequence of thin plates with a gap between them commensurable with the photon formation length

$$l_{\mathrm{f}} = \frac{2E_e}{m_e^2 c^3}\left(\frac{E_e}{\omega} - \hbar\right). \tag{1}$$

The latter length depends on the electron energy E_e and the photon energy $\hbar\omega$ in the window covered by the detector (m_e being the electron mass). The problem of a structured target as applied to small-angle emission of gamma quanta was pioneered by Blankenbecler [14,15], who treated it on the basis of a model for multiple scattering proposed in [6]. Other authors [7,16] then extended their formalisms to handle this problem.

An experimental verification of the existence of interference effects in bremsstrahlung on compound targets has recently been undertaken at CERN [17–19]. It was pointed out [18,19] that high electron energy can render the photon formation length (1) macroscopic and allow to study its manifestations by variation of the distance between the scattering plates with a micrometer screw. But even for CERN SPS energies, $E_e \approx 178$ GeV, the coefficient in Eq. (1) amounts only to $\frac{2E_e}{m_e^2 c^3} \approx 0.3\ \mu\mathrm{m}/\hbar$, wherefore in order to make l_{f} instrumentally macroscopic ($\gtrsim 10\ \mu$m), one needs to deal with sufficiently small photon energies compared to E_e, rendering the problem essentially classical. At the same time, condition $\omega/E_e \gg 10^{-4}$ can still be satisfied, wherewith the contribution from transition radiation keeps negligible. Experiment [19] conducted under such conditions favored theory [14], but found some departures from it, as well as from other theoretical predictions, which were expected to be more accurate.

To explain the origin of the remaining discrepancies, let us recollect underlying assumptions for the theories at the market. Blankenbecler and Drell [6] in essence extended Landau and Pomeranchuk's approach [2] to cover the case of a finite-thickness target and to allow for quantum effects. At that, a simplified model of scattering in a medium was adopted, in which transverse dimensions of the target random field exceeded that of the electron wave packet, enabling exact integration over electron impact parameters and reduction of the photon emission amplitude to an integral over the particle trajectory, like in *classical mechanics*. A strong simplification was made thereupon, in the spirit of [2], by replacing the medium average of an oscillatory integrand by the corresponding oscillatory function of averaged variables. That yielded the angle-integral spectrum in the form of a double time integral, which for most cases of interest had to be computed numerically. Along these lines, Blankenbecler [14] evaluated the spectrum of radiation on N plates and discovered an additional maximum, or "shoulder," in the region where the gap width becomes commensurable with the radiation coherence length.

The approach of Blankenbecler and Drell has the merit of being simple and qualitatively correct. However, it lacks accuracy due to the oversimplification of averaging (the neglect of fluctuations), which may become essential when

*bon@kipt.kharkov.ua

bringing the theory into comparison with experiment. In his later paper [15], Blankenbecler took into account also a correlation of the amplitude and the phase of the integrand in the double time integral, while other fluctuations were neglected, as before. We will show below, however, that this correction alone improves the accuracy for the case of weak scattering in the plates only, while in the opposite case of strong (nondipole) scattering, in which interference effects are actually the strongest, this correction is not helpful.

Almost simultaneously with [6,14], Zakharov [7] delivered a calculation of the LPM effect in finite targets with a rigorous (Molière) treatment of the averaging. It utilized techniques originally developed for particle physics, notably the impact parameter representation, having the advantage of naturally invoking Fourier transforms of scattering-angle distribution functions, which from solution of the kinetic equation express as simple exponentials of the Fourier-transformed scattering differential cross section. The main attention in papers [7] was paid to a single finite-thickness target, while for a structured target, the results were presented only graphically. Zakharov found the interference features in his calculated spectrum to be less pronounced than those in [14], but attributed that to the crudeness of the Blankenbecler-Drell model for the scattering medium, rather than to an oversimplification of their averaging procedure.

Shortly after, Baier and Katkov [16] advanced with a technique allowing them to handle the case of N scattering plates analytically. To this end, an alternative form of the double time integral representation for the radiation spectrum was used, and radiation spectra for N plates were calculated by mathematical induction, assuming all the plates to be identical, equidistant, and the scattering angle distributions in them to be Gaussian. The influence of the transition radiation was taken into account, as well, which can be valuable for lower-energy experiments. Baier and Katkov ultimately restricted their analysis to the case of plates infinitesimally thin compared to the gap width, and demonstrated that instead of one maximum, the radiation spectrum features a sequence of maxima and minima of decreasing amplitude.

The common drawback shared by all the abovementioned approaches is that the resulting expressions for the radiation spectrum are given by rather bulky integrals, and relations of the spectral features with physical parameters in the problem are not transparent. In fact, that even led to a number of qualitative controversies in the literature, most noticeable among which are the following:

(i) It was suggested in [14] that the position of the largest spectral maximum corresponds to a situation when the photon formation length (1) matches the distance between the plate centers. In that case, however, the resonance condition ought to involve an additional factor 2π, as in coherent bremsstrahlung (see [19,20]). But then it would drastically contradict the experiment [19].

(ii) In integral representations of the radiation spectrum, the argument of the oscillatory function typically is $\frac{\omega t}{2\gamma^2}(1+\gamma^2\theta^2)$, where γ is the electron's Lorentz factor, and θ the radiation angle. Therewith, if the distance between the plate centers equals ct_{21}, the main spectral maximum should be located at

$$\omega \simeq 2\pi \frac{2\gamma^2}{t_{21}(1+\gamma^2\theta^2)},$$

involving factor 2π, as expected, but also a denominator $1+\gamma^2\theta^2$, tending to compensate it. Yes it is not *a priori* obvious with respect to which direction the radiation angles should be counted and how large their typical values are. If one estimates them as $\theta \sim \max\{\gamma^{-1}, \sigma\}$, where σ is the rms scattering angle in the plates [16], then for $\sigma \gg \gamma^{-1}$ the compensation between the 2π factor and the denominator can be substantial. But still such estimates numerically contradict the experimental findings [19].

Given fundamental significance of the present problem on the one hand, and apparent uncertainties and contradictions in the theoretical predictions on the other hand, it seems timely to examine more closely the experimentally addressed case of two scattering plates, and fully exploit the simplicity of its geometry. For this case, it appears possible to derive physically more transparent representations for the radiation spectrum, which help elucidate the matter as a whole. To alleviate the mathematical problem, we will consider two *geometrically thin* scattering plates (foils), which lifts the necessity to use double time integral representations for the radiation spectrum. We will also limit ourselves to classical electrodynamics, and neglect the transition radiation, which is admissible under conditions of experiments [17–19]. On the other hand, we shall include a more detailed investigation of the influence of Coulomb nature of multiple scattering, as long as approaches of Baier and Katkov, as well as Blankenbecler and Drell, were restricted to Gaussian description of scattering. To facilitate the connection between the theory and experiment, our conclusions will be cast in terms of appropriate visibilities of the interference pattern. The controversies mentioned above will be resolved, and several errors existing in the literature will be fixed. Ultimately, we compare our predictions with the recent experimental data, and show that there is no significant discrepancy between the experiment and the theory.

II. GENERIC SPECTRUM OF RADIATION AT TWO SCATTERINGS

In classical electrodynamics, the spectral-angular energy distribution of radiation (with the direction of photon emission denoted by vector $\boldsymbol{n}$) expresses through the

charged particle trajectory $\boldsymbol{r}(t)$, $\boldsymbol{v}(t) = d\boldsymbol{r}/dt$ in a known way [21]:

$$\frac{dI}{d\omega d^2n} = \frac{e^2}{c}\left|\frac{1}{2\pi}\int_{-\infty}^{\infty} dt e^{i\omega[t-\boldsymbol{n}\cdot\boldsymbol{r}(t)/c]}\frac{d}{dt}\frac{\boldsymbol{n}\times\boldsymbol{v}(t)}{c-\boldsymbol{n}\cdot\boldsymbol{v}(t)}\right|^2, \quad (2)$$

e being the electron charge, and c the speed of light. For our present study, it will be sufficient to consider a simple case when the electron experiences two abrupt scatterings, at instants t_1 and t_2:

$$\boldsymbol{v}_1 \underset{t_1}{\rightarrow} \boldsymbol{v}_2 \underset{t_2}{\rightarrow} \boldsymbol{v}_3.$$

Integration over time in Eq. (2) then trivially yields

$$\frac{dI}{d\omega d^2n} = \frac{e^2}{4\pi^2 c}|\boldsymbol{n}\times\boldsymbol{J}_{21} + \boldsymbol{n}\times\boldsymbol{J}_{32}e^{i\Psi}|^2 \quad (3a)$$

$$= \frac{e^2}{4\pi^2 c}[(\boldsymbol{n}\times\boldsymbol{J}_{21})^2 + (\boldsymbol{n}\times\boldsymbol{J}_{32})^2 + 2(\boldsymbol{n}\times\boldsymbol{J}_{21})\cdot(\boldsymbol{n}\times\boldsymbol{J}_{32})\cos\Psi], \quad (3b)$$

with

$$\boldsymbol{J}_{21}(\boldsymbol{n}) = \frac{\boldsymbol{v}_1}{c-\boldsymbol{n}\cdot\boldsymbol{v}_1} - \frac{\boldsymbol{v}_2}{c-\boldsymbol{n}\cdot\boldsymbol{v}_2}, \quad (4)$$

$$\boldsymbol{J}_{32}(\boldsymbol{n}) = \frac{\boldsymbol{v}_2}{c-\boldsymbol{n}\cdot\boldsymbol{v}_2} - \frac{\boldsymbol{v}_3}{c-\boldsymbol{n}\cdot\boldsymbol{v}_3}, \quad (5)$$

$$\Psi(\omega,\boldsymbol{n}) = \omega(t_2-t_1)(1-\boldsymbol{n}\cdot\boldsymbol{v}_2/c). \quad (6)$$

Equation (3a) demonstrates that for well separated scatterings, the spectral radiation amplitude can be viewed as a sum of spectral amplitudes of radiation at single scatterings (with a distance- and ω-dependent phase shift Ψ between them). In each of such amplitude terms, there are no effects of the electron's proper field distortion between scatterings. However, observed in practice is the radiation intensity, being proportional to the square of the full amplitude, and it differs from the sum of intensities of radiation on separate foils. Also, it engages a certain dependence on ω through the cosine of the phase shift between the foils.

An important generic property of Eq. (3b) is that the ω integral of the interference term therein strictly vanishes:

$$\int_0^\infty d\omega\left(\frac{dI}{d\omega d^2n} - \frac{dI_1}{d\omega d^2n} - \frac{dI_2}{d\omega d^2n}\right) \equiv 0,$$

by virtue of the relation

$$\int_0^\infty d\omega\cos\Psi = \pi\delta[t_{21}(1-\boldsymbol{n}\cdot\boldsymbol{v}_2/c)], \quad (7)$$

and nonzero value of the argument of the δ function if $t_{21} = t_2 - t_1 \neq 0$. The absence of interference in the total classical radiative energy loss can be traced to the absence of spatial overlap and temporal correlation between the scatterings (as discussed in application to LPM effect by [22]).

Another important point is that for bremsstrahlung in a sufficiently thin layer of substance, typical scattering angles are small compared to γ^{-1} (the dipole limit):

$$(\boldsymbol{v}_2-\boldsymbol{v}_1)^2/c^2 \ll 1 - v^2/c^2 = \gamma^{-2}.$$

In that case, the structure of currents (4)–(5) appreciably simplifies. Linearizing $\boldsymbol{J}_{21}$ in $(\boldsymbol{v}_2-\boldsymbol{v}_1)/c = \boldsymbol{\chi}_1$ and $\boldsymbol{J}_{32}$ in $(\boldsymbol{v}_3-\boldsymbol{v}_2)/c = \boldsymbol{\chi}_2$, then integrating (3b) over radiation angles, and averaging over scattering angles $\boldsymbol{\chi}_1, \boldsymbol{\chi}_2$ yields

$$\left\langle\frac{dI}{d\omega}\right\rangle = \left(\left\langle\frac{dI_1}{d\omega}\right\rangle + \left\langle\frac{dI_2}{d\omega}\right\rangle\right)\left[1 + \frac{2\langle\boldsymbol{\chi}_1\cdot\boldsymbol{\chi}_2\rangle}{\langle\boldsymbol{\chi}_1^2\rangle + \langle\boldsymbol{\chi}_2^2\rangle}g_{\rm dd}(\Omega)\right], \quad (8)$$

with

$$g_{\rm dd}(\Omega) = \frac{3}{2}\int_0^\infty d\Theta^2\frac{1+\Theta^4}{(1+\Theta^2)^4}\cos\Omega(1+\Theta^2), \quad (9)$$

$$\Omega = \frac{\omega t_{21}}{2\gamma^2} \equiv \frac{ct_{21}}{l_{\rm f}(\omega)}, \quad (10)$$

and

$$\Theta = \gamma\theta. \quad (11)$$

If consecutive scatterings are causally disconnected, the correlator in (8) reduces to a product of mean scattering angles:

$$\langle\boldsymbol{\chi}_1\cdot\boldsymbol{\chi}_2\rangle = \langle\boldsymbol{\chi}_1\rangle\cdot\langle\boldsymbol{\chi}_2\rangle.$$

For amorphous targets, mean deflection angles are zero, wherefore the whole interference in the spectrum vanishes in the given approximation. To maintain the interference effects between the targets, one thus needs either to make both scatterings asymmetric,[1] or to arrange *nondipole* conditions for radiation in the amorphous target; the latter may be easier to fulfill in practice and will be the subject of our following study.

III. SPECTRUM OF NONDIPOLE RADIATION FROM ONE FOIL

Before addressing interference effects in a composite target, let us recapitulate the properties of bremsstrahlung on a single amorphous foil, and highlight the differences

[1]Natural candidates for such deflectors could be magnets, but strong magnets with dimensions smaller than $l_{\rm f}$, for ω in the gamma range, are challenging to manufacture. More compact deflectors could be created with the aid of lasers, as proposed in [18], or bent crystals.

between approaches of different authors. Aiming to reach a reasonable balance between simplicity and numerical accuracy, in this section we will also consider both Gaussian and Molière averaging procedures, and derive a simple relation of the Coulomb screening effects with the radiation length.

The radiation spectrum at electron scattering through a definite angle (which at high energy is usually small, but may be sizable compared to the typical radiation angle γ^{-1}) is given by an integral over photon emission angles (see, e.g., [23])

$$\frac{dI_1}{d\omega} = \frac{e^2}{4\pi^2 c}\int d^2n(\boldsymbol{n}\times\boldsymbol{J}_{21})^2 = \frac{2e^2}{\pi c}F(\gamma\chi/2), \tag{12}$$

where χ is the electron's scattering angle, and

$$F(\xi) = \frac{2\xi^2+1}{\xi\sqrt{\xi^2+1}}\ln(\xi+\sqrt{\xi^2+1}) - 1. \tag{13}$$

Small-angle expansion of (13) to all orders can be obtained as

$$F(\xi) = -\sum_{n=1}^{\infty}\frac{(n-1)!(n+1)!}{(2n+1)!}(-4\xi^2)^n \tag{14a}$$

$$= \frac{4}{3}\xi^2 - \frac{4}{5}\xi^4 + \ldots = \frac{1}{3}(\gamma\chi)^2 - \frac{1}{20}(\gamma\chi)^4 + \ldots. \tag{14b}$$

Series (14a) has a finite (actually, unit) convergence radius, due to the presence in (13) of the branching $\sqrt{\xi^2+1}$.

The large-angle asymptotics of (13) is logarithmic:

$$F(\xi) \underset{\xi\to\infty}{\simeq} 2\ln 2\xi - 1 = 2\ln\gamma\chi - 1. \tag{15}$$

Physically, the logarithm here originates from the fact that although for a large-angle scattering, the radiation cones from the initial and final electron lines are well separated, the region between them is filled by an enhanced radiation, due to the interference between the cones. The integration over this interjet domain gives rise to the large logarithm in Eq. (15).

A. Gaussian averaging over scattering angles

Equations (12), (13) may be used to derive the radiation spectrum in a geometrically thin layer of substance, i.e., when the target thickness is much smaller than the photon formation length (1) in the considered range of ω. To this end, Eq. (12) must be convolved with the appropriate distribution in scattering angles in the target [4,9]. In the simplest approximation, this distribution can be taken to be Gaussian. Averaging over scattering angles with the Gaussian probability distribution

$$\frac{dw_\sigma}{d\chi^2} = \frac{1}{\sigma^2}e^{-\chi^2/\sigma^2}, \tag{16}$$

where σ is the rms scattering angle, gives

$$\left\langle\frac{dI_1}{d\omega}\right\rangle_\sigma = \frac{2e^2}{\pi c}\langle F\rangle_\sigma, \tag{17}$$

with

$$\langle F\rangle_\sigma = \int_0^\infty d\chi^2\frac{1}{\sigma^2}e^{-\chi^2/\sigma^2}F(\gamma\chi/2) = \frac{8}{\gamma^2\sigma^2}\int_0^\infty d\xi\xi e^{-\frac{4\xi^2}{\gamma^2\sigma^2}}F(\xi). \tag{18}$$

Plugging here (14a) and integrating termwise yields

$$\langle F\rangle_\sigma = -\sum_{n=1}^{\infty}\frac{(n-1)!n!(n+1)!}{(2n+1)!}(-\Sigma^2)^n, \tag{19}$$

with

$$\Sigma = \gamma\sigma. \tag{20}$$

Series (19) diverges for any finite Σ (as long as it has been derived by integrating a series beyond its convergence domain), but nonetheless, the sequence of its terms may be used as an asymptotic expansion.

The first two terms in Eq. (19) read

$$\langle F\rangle_\sigma \underset{\Sigma\ll 1}{\simeq} \frac{1}{3}\Sigma^2 - \frac{1}{10}\Sigma^4. \tag{21}$$

Note that the coefficient at the leading-order term is the same as in (14b), whereas the coefficient at the next-to-leading order term is twice greater.

To obtain large-Σ asymptotics of $\langle F\rangle_\sigma$, one can change in (18) the integration variable to $\xi = \sinh\frac{w}{2}$:

$$\langle F\rangle_\sigma = \frac{2}{\Sigma^2}e^{\frac{2}{\Sigma^2}}\int_0^\infty dwe^{-\frac{2}{\Sigma^2}\cosh w}w\cosh w - 1 = e^{\frac{2}{\Sigma^2}}K_0\left(\frac{2}{\Sigma^2}\right) - 1 + \frac{2}{\Sigma^2}e^{\frac{2}{\Sigma^2}}\int_0^\infty dwwe^{-w-\frac{2}{\Sigma^2}\cosh w}. \tag{22}$$

The remaining integral in (22) is a bounded function, ranging from 0 to 1. At large Σ, that term vanishes due to the prefactor Σ^{-2}, so the corresponding asymptotics of $\langle F\rangle_\sigma$ is determined by that of the Macdonald function at the origin: $K_0(z) \underset{z\to 0}{\simeq} \ln\frac{2}{z} - \gamma_E$, with $\gamma_E = 0.577$ the Euler constant. Employing this in (22), we get [9]

$$\langle F\rangle_\sigma \underset{\Sigma\gg 1}{\simeq} 2\ln\Sigma - \gamma_E - 1. \tag{23}$$

B. Blankenbecler's approximations

At this point, it is worth comparing the result (17)–(18) with representations derived by Blankenbecler [14], and Baier and Katkov [16], under the same conditions of geometrically thin target and Gaussian scattering.

Blankenbecler's result [see [14], Eq. (30)] for the thin-target limit expresses as

$$F_{\rm B}(T)=\int_0^1 dw\left(\frac{1+3T}{1+6Tw(1-w)}-1\right), \tag{24a}$$

where the dimensionless parameter T is proportional to the target thickness. Evaluation of integral (24a) yields

$$F_{\rm B}(T)=F(\sqrt{3T/2}), \tag{24b}$$

where F is given by Eq. (13). Hence, the correspondence between T and Σ should read

$$T=\Sigma^2/6, \tag{25}$$

and the Blankenbecler's approximation amounts to replacing in the *nonaveraged* (fixed-scattering-angle) radiation spectrum [(12)] the scattering angle χ by the rms scattering angle σ:

$$F_{\rm B}(T)=F(\Sigma/2). \tag{26}$$

This correspondence is what one should expect, as long as Blankenbecler and Drell [6], similarly to Landau and Pomeranchuk [2], adopted a simplification of replacing the average of an oscillatory function in the integrand of a double time integral by the oscillatory function with average amplitude and phase. As is evident from Fig. 1(a), though, in the present case such a "thermodynamic" approximation deviates from the exact result only by ∼15%.

Yet another source of inaccuracy, however, may arise due to the fact that for numerical calculations, Blankenbecler adopted a simplified relation for the mean square transverse momentum acquired by the electron in the target:

$$\langle Q_\perp^2\rangle=\frac{2\pi m_e^2c^2}{\alpha}\frac{l}{X_0} \tag{27}$$

(l being the target thickness, X_0 the radiation length, and $\alpha=e^2/\hbar c=1/137$). The coefficient in (27) differs by a constant factor $1/2$ from that in the Rossi formula [24]

$$\langle Q_\perp^2\rangle=\frac{4\pi m_e^2c^2}{\alpha}\frac{l}{X_0}. \tag{28}$$

Correspondingly, Blankenbecler defined the scaled target thickness [see [6], Eq. (10.1), [14], Eq. (16)]

$$T=\frac{\pi}{3\alpha}\frac{l}{X_0},$$

consistent with the correspondence rule (25). But physically, the situation must be more complicated, as long as the coefficient in the relation between $\langle Q_\perp^2\rangle$ and l/X_0 varies with l logarithmically. A more accurate description of multiple Coulomb scattering will be delivered in Sec. III D.

In [15], Blankenbecler calculated a correction to Eq. (24a) [see [15], Eq. (109)], reading

$$\tilde F_{\rm B}(T)=\int_0^1 dw\left\{\frac{1+\frac{3}{2}T}{1+6Tw(1-w)}+\frac{\frac{3}{2}T}{[1+6Tw(1-w)]^2}-1\right\}. \tag{29}$$

At small T, i.e., small Σ, it almost exactly reproduces the next-to-leading order term in small-angle expansion (21), provided one uses here the correspondence rule (25):

$$\tilde F_{\rm B}(T)\underset{\Sigma\ll1}{\simeq}2T-\frac{33}{10}T^2=\frac{1}{3}\Sigma^2-\frac{11}{120}\Sigma^4. \tag{30}$$

However, at large Σ (or T), approximation (29) departs from the exact result by a factor of 2 [see Fig. 1(a), red dot-dashed curve] and thus cannot be regarded as everywhere valid.

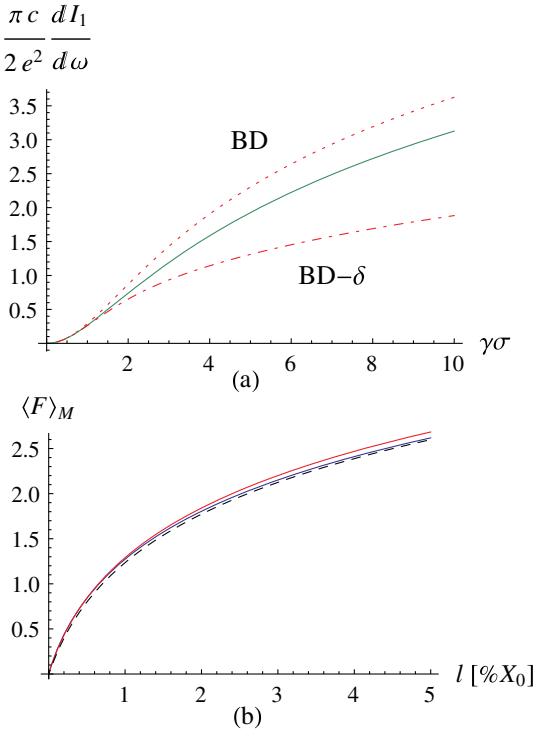

FIG. 1 (color online). (a) Green solid curve, $\langle F\rangle_\sigma$ [Eq. (18) or (37)]; red dashed curve, F [Eq. (13) or (26)]; red dot-dashed curve, the corrected Blankenbecler-Drell approximation (29). (b) Red curve (upper), Molière averaging for gold; blue curve, Molière averaging for carbon; dashed curve, Gaussian averaging with the use of Eq. (45).

C. Baier and Katkov's representation

Baier and Katkov within their framework [16] obtained for the case of one foil the form factor[2]

$$F_{\mathrm{BK}}(b)=\int_0^\infty \frac{dx}{x}e^{-x}\int_0^1 dw\left\{1-\frac{1}{[1+\frac{x}{b}w(1-w)]^2}\right\}. \tag{31}$$

Evaluation of the latter integral recovers expression (18), once one identifies

$$b=\Sigma^{-2}. \tag{32}$$

That leads to the correspondence rule

$$F_{\mathrm{BK}}(\Sigma^{-2})=\langle F\rangle_\sigma.$$

Thus, Baier-Katkov's procedure corresponds to proper Gaussian averaging.

D. Weighting with the Molière distribution: Impact parameter representation

For physically very thin targets, the distribution in scattering angles must ultimately deviate from a Gaussian, in the extreme $l\to 0$ becoming proportional to the differential cross section of scattering on one atom. To allow for this possibility, as well as gain better accuracy in general, one may utilize the exact (Molière) solution of the kinetic equation in terms of a Fourier-Bessel integral [25]:

$$\frac{dw_{\mathrm{M}}}{d^2\chi}=\frac{1}{(2\pi)^2}\int d^2\xi e^{i\boldsymbol{\xi}\cdot\boldsymbol{\chi}}e^{-nl\int d\sigma(\chi)[1-J_0(\xi\chi)]}. \tag{33}$$

Here $d\sigma(\chi)$ is the electron-atom scattering differential cross section, and n the density of atoms in the medium. At substantial thicknesses, integral (33) is often approximated by a Gaussian plus a single-scattering correction [25], but we will not resort to such an approximation herein, dealing directly with integral representation (33).

Issuing from Eqs. (3), (4), the spectrum of radiation at one scattering can be rewritten as

$$\begin{aligned}\frac{dI_1}{d\omega}&=\frac{e^2}{4\pi^2 c}\int d^2n\left(\frac{\boldsymbol{n}\times\boldsymbol{v}_1}{c-\boldsymbol{n}\cdot\boldsymbol{v}_1}-\frac{\boldsymbol{n}\times\boldsymbol{v}_2}{c-\boldsymbol{n}\cdot\boldsymbol{v}_2}\right)^2\\&=\frac{e^2}{4\pi^2 c}\int d^2n\left[\frac{\boldsymbol{n}-\boldsymbol{v}_1/c}{\gamma^{-2}+(\boldsymbol{n}-\boldsymbol{v}_1/c)^2}-\frac{\boldsymbol{n}-\boldsymbol{v}_2/c}{\gamma^{-2}+(\boldsymbol{n}-\boldsymbol{v}_2/c)^2}\right]^2,\end{aligned} \tag{34}$$

where the last integral effectively extends over the transverse plane of small angle differences. Observing that the two terms in brackets in (34) only differ by a shift in the $\boldsymbol{n}_\perp$ plane, it may be expedient to expand them into Fourier integrals, wherewith the angular shift converts to a phase factor:

$$\frac{\boldsymbol{n}-\boldsymbol{v}/c}{\gamma^{-2}+(\boldsymbol{n}-\boldsymbol{v}/c)^2}=\frac{i}{2\pi}\int d^2\xi e^{i(\boldsymbol{n}-\boldsymbol{v}/c)\cdot\boldsymbol{\xi}}\frac{\partial}{\partial\boldsymbol{\xi}}K_0(\xi/\gamma). \tag{35}$$

Since $\frac{\hbar\omega}{c}(\boldsymbol{n}-\boldsymbol{v}/c)$ is the photon's transverse momentum, its Fourier conjugate $c\boldsymbol{\xi}/\omega$ can be interpreted as the photon's impact parameter relative to the parent electron.

Inserting (35) into Eq. (34) gives

$$\frac{dI_1}{d\omega}=\frac{e^2}{\pi^2 c}\int d^2\xi\left[\frac{\partial}{\partial\boldsymbol{\xi}}K_0(\xi/\gamma)\right]^2|1-e^{i(\boldsymbol{v}_1-\boldsymbol{v}_2)\cdot\boldsymbol{\xi}/c}|^2 \tag{36a}$$

$$=\frac{4e^2}{\pi c}\int_0^\infty d\rho\rho K_1^2(\rho)[1-J_0(\rho\gamma\chi)], \tag{36b}$$

where for convenience we rescaled the impact parameter variable to $\rho=\xi/\gamma$. It can be checked that evaluation of the integral in (36b) reproduces the explicit form (12), (13).

From the viewpoint of light-cone formalism [26], $\frac{e}{\pi\sqrt{c\hbar\omega}}\frac{\partial}{\partial\boldsymbol{\xi}}K_0(\xi/\gamma)$ can be interpreted as (the low-ω limit for) the electron-photon component of the electron wave function, with the vector index accounting for the photon polarization. In this spirit, $\frac{e}{\pi\sqrt{c\hbar\omega}}\frac{\partial}{\partial\boldsymbol{\xi}}K_0(\xi/\gamma)(1-e^{i(\boldsymbol{v}_1-\boldsymbol{v}_2)\cdot\boldsymbol{\xi}/c})$ may be viewed as the corresponding Fock component after electron scattering through a definite angle; this wave function differs from zero for $\boldsymbol{v}_2\neq\boldsymbol{v}_1$. Correspondingly, the integral of its modulus square gives the total probability of emission of a photon with energy ω, i.e., the radiation spectrum. Interpretations of that kind may be instructive for understanding of the final results, albeit in this paper we will not embark on them technically, adhering to the standard formulation of classical electrodynamics.[3]

To proceed, when expression (36b) is averaged over scattering angles with the Gaussian distribution (16), it assumes the form

$$\begin{aligned}\left\langle\frac{dI_1}{d\omega}\right\rangle_\sigma&=\int d^2\chi\frac{dw_\sigma}{d^2\chi}\frac{dI_1}{d\omega}\\&=\frac{4e^2}{\pi c}\int_0^\infty d\rho\rho K_1^2(\rho)(1-e^{-\rho^2\gamma^2\sigma^2/4}).\end{aligned} \tag{37}$$

On the other hand, averaging with Molière distribution (33) leads to

$$\left\langle\frac{dI_1}{d\omega}\right\rangle_{\mathrm{M}}=\frac{4e^2}{\pi c}\int_0^\infty d\rho\rho K_1^2(\rho)\{1-e^{-nl\int d\sigma(\chi)[1-J_0(\rho\gamma\chi)]}\}, \tag{38}$$

[2]We restored factor x^{-1} missing in [16].

[3]Thereby, we also encounter no "vacuum" divergences, compared with approaches [6,7,14,16] where subtraction of divergent vacuum terms from the final result was needed.

essentially coinciding with the result of Zakharov [7] (see also [8]).[4]

To use formula (38), next one needs to specify the atomic differential scattering cross section. Its most essential feature is the Rutherford asymptotics at large χ, which in the Bethe-Molière theory is expressed as

$$nld\sigma(\chi) = 2\chi_c^2 \frac{\chi d\chi}{\chi^4} q(\chi),$$

where for ultrarelativistic particles

$$\chi_c^2 = 4\pi Z(Z+1)\alpha^4 a_B^2 nl\gamma^{-2},$$

and $q(\chi)$ is a monotonous function with asymptotic properties $q(\chi) \underset{\chi\gg\chi_1}{\to} 1$, $\chi^{-4}q(\chi) \underset{\chi\ll\chi_1}{\to}$ const. Physically, scale χ_1 is smaller than γ^{-1}, because $\gamma\chi_1 \sim \frac{\hbar}{m_e cR} = \alpha\frac{a_B}{R} \ll 1$, where a_B is the Bohr radius and R the atomic screening radius. Parameter ρ effectively cannot be large, because in the integral over ρ, the overall factor $K_1^2(\rho)$ exponentially vanishes for large transverse separations ρ. Hence, in the integral in the exponent of Eq. (38) there exists an interval $\chi_1 \ll \chi \ll \frac{1}{\rho\gamma}$, where one can set $q \approx 1$, $1 - J_0(\rho\gamma\chi) \approx \frac{1}{4}\rho^2\gamma^2\chi^2$, and the integrand scales as $nld\sigma(\chi)[1 - J_0(\rho\gamma\chi)] \sim \frac{1}{2}\rho^2\gamma^2\chi_c^2\frac{d\chi}{\chi}$, giving a large logarithmic contribution. Evaluating the integral to the next-to-leading logarithmic approximation (in exactly the same way as in the Bethe-Molière multiple scattering theory [25]), one gets

$$\left\langle \frac{dI_1}{d\omega} \right\rangle_M = \frac{4e^2}{\pi c}\int_0^{\sim\alpha^{-1}} d\rho\rho K_1^2(\rho)\left\{1 - e^{-\frac{1}{2}\rho^2\gamma^2\chi_c^2\left(\ln\frac{2}{\gamma\chi_1\rho}+\frac{1}{2}-\gamma_E\right)}\right\}, \tag{39}$$

where

$$\ln\chi_1 = \int_0^\infty d\chi \frac{dq}{d\chi}\ln\chi - \frac{1}{2}$$

is the conventional definition for the screening angle at single scattering [25].

The value of χ_1 is often evaluated based on the Thomas-Fermi model, but to reach satisfactory precision, one needs to separately treat radiation with and without atom ionization, characterized by different screening radii [28,29]. Still, such a calculation does not account for interatotic electron redistribution effects, such as covalent bonds, collective electrons in metals, etc. An alternative approach may be to regard $\gamma\chi_1$ as a purely phenomenological parameter and relate it to another, more directly measurable observable, such as the radiation length for the given material. That would reduce the theoretical uncertainty as well as the complexity of calculations. To this end, observe that in the limit of small l, the radiation spectrum tends to

$$\left\langle \frac{dI_1}{d\omega} \right\rangle_M \underset{l\to 0}{\simeq} \frac{2e^2\gamma^2\chi_c^2}{\pi c}\int_0^\infty d\rho\rho^3 K_1^2(\rho)\left(\ln\frac{2}{\rho\gamma\chi_1} + \frac{1}{2} - \gamma_E\right) \tag{40a}$$

$$\equiv \frac{4e^2\gamma^2\chi_c^2}{3\pi c}\left(\ln\frac{1}{\gamma\chi_1} + \frac{7}{12}\right). \tag{40b}$$

On the other hand, by the definition of the radiation length (in the approximation of complete screening), that must equal[5]

$$\frac{1}{\hbar}\left\langle \frac{dI_1}{d\omega} \right\rangle_M \underset{l\to 0}{\simeq} \frac{4l}{3X_0}. \tag{41}$$

Hence, parameter χ_1 is related with the product of measurable quantities n and X_0 via

$$\gamma\chi_1 = \exp\left(\frac{7}{12} - \frac{1}{4Z(Z+1)\alpha^5 a_B^2 nX_0}\right). \tag{42}$$

In this paper, our approach will be simply to employ relation (42) in conjunction with the equation providing a smooth cutoff at large ρ [corresponding to the model for the regulating function $q(\chi) = (1+\chi_1^2/\chi^2)^{-2}$]:

$$\left\langle \frac{dI_1}{d\omega} \right\rangle_M = \frac{4e^2}{\pi c}\int_0^\infty d\rho\rho K_1^2(\rho)\left\{1 - e^{-\frac{\chi_c^2}{\chi_1^2}[1-\rho\gamma\chi_1 K_1(\rho\gamma\chi_1)]}\right\}. \tag{43}$$

The factor $\frac{\chi_c^2}{\chi_1^2}$ in the exponent expresses in terms of the ratio l/X_0:

$$\frac{\chi_c^2}{\chi_1^2} = \frac{\pi}{\alpha\gamma^2\chi_1^2(\ln\frac{1}{\gamma\chi_1}+\frac{7}{12})}\frac{l}{X_0}. \tag{44}$$

It may be noted, however, that in practice, X_0 itself is often inferred from calculations by formulas for bremsstrahlung on an isolated atom, neglecting the above mentioned interatomic effects as a whole [11,28,30]. In that case, our approach offers more simplicity, but may be unable to provide greater accuracy.

[4]This is also in the spirit of Glauber's form [27] for scattering of a high-energy composite quantum system. (It is not crucial in our case that the scattering is multiple, since the impact parameter is conserved, anyway.)

[5]Corrections to the complete screening approximation might be taken into account via a redefinition of X_0 in Eq. (41).

Regarding our relation of multiple scattering with the radiation length, it may also be noted that there is another widely used engineering formula [30,31][6]:

$$\gamma\sigma = \frac{13.6\ \mathrm{MeV}}{m_e c^2}\sqrt{\frac{2l}{X_0}}\left(1 + 0.038\ln\frac{l}{X_0}\right) \tag{45}$$

relating the effective rms scattering angle σ with the l/X_0 ratio. It is asserted that formula (45) works with an accuracy better than 10% for $l > 10^{-3}X_0$. In fact, formula (45) can be derived from the rigorous representation (39), as is shown in the Appendix.

It is nonetheless instructive to compare predictions based on Eq. (45) and our Eq. (42) numerically. Figure 1(b) overlays the predictions of Eqs. (42), (43) for carbon and gold, and also the form factor (18) for Gaussian averaging with σ evaluated by formula (45). We see that for bremsstrahlung on one plate, the agreement is good in the whole range of l, including $l < 10^{-3}X_0$.

IV. TWO FOILS: RESULTS

We are now in a position to address the case of two scattering plates. In Eq. (3b), the first two terms are individual contributions from each plate, described by formulas of Sec. III, while the third term of Eq. (3b) containing all the interference effects involves the product of currents induced by scatterings in different plates. Hence, averaging of those currents over corresponding scattering angles proceeds independently:

$$\langle(\boldsymbol{n}\times\boldsymbol{J}_{21})\cdot(\boldsymbol{n}\times\boldsymbol{J}_{32})\rangle = (\boldsymbol{n}\times\langle\boldsymbol{J}_{21}\rangle)\cdot(\boldsymbol{n}\times\langle\boldsymbol{J}_{32}\rangle). \tag{46}$$

As was pointed out in the end of Sec. II, product (46) may receive significant suppression after integration over azimuthal directions of $\boldsymbol{n}$. Therefore, it is reasonable to split the averaging in two steps: First, average the currents over azimuths of the scattering angles, which needs no reference to a specific form of the (axially symmetric) scattering angle distribution function. The second step is to convolve the currents with specific angular distribution functions.

A. Azimuthal averaging for the interference term

Granted that the currents entering Eq. (3) have similar structure, it suffices to consider a generic vector amplitude

$$\boldsymbol{J} = \frac{\boldsymbol{v}_2}{c - \boldsymbol{n}\cdot\boldsymbol{v}_2} - \frac{\boldsymbol{v}}{c - \boldsymbol{n}\cdot\boldsymbol{v}}, \tag{47}$$

where $\boldsymbol{v}$ may equal $\boldsymbol{v}_1$ or $\boldsymbol{v}_3$. Averaging of expression (47) over azimuths of the scattering angle can be carried out under the fixed direction $\boldsymbol{v}_2$; that makes no difference, as long as ultimately all directions are to be integrated over. Decomposing $\boldsymbol{v}$ into components parallel and orthogonal to $\boldsymbol{v}_2$,

$$\boldsymbol{v} = \boldsymbol{v}_\parallel + \boldsymbol{v}_\perp, \tag{48}$$

with $\boldsymbol{v}_\perp \perp \boldsymbol{v}_2 \| \boldsymbol{v}_\parallel$, one computes the azimuthal average:

$$\begin{aligned}\left\langle\frac{\boldsymbol{v}_\parallel + \boldsymbol{v}_\perp}{c - n_\parallel v_\parallel - \boldsymbol{n}_\perp\cdot\boldsymbol{v}_\perp}\right\rangle_{\mathrm{azim}\,\boldsymbol{v}_\perp} &\equiv \frac{1}{2\pi}\int_{-\pi}^{\pi} d\phi\,\frac{\boldsymbol{v}_\parallel + \frac{\boldsymbol{n}_\perp}{n_\perp}v_\perp\cos\phi}{c - n_\parallel v_\parallel - n_\perp v_\perp\cos\phi} \\ &= \frac{\boldsymbol{v}_\parallel + \frac{\boldsymbol{n}_\perp}{n_\perp^2}(c - n_\parallel v_\parallel)}{\sqrt{(c - n_\parallel v_\parallel)^2 - n_\perp^2 v_\perp^2}} - \frac{\boldsymbol{n}_\perp}{n_\perp^2}.\end{aligned} \tag{49}$$

Inserting here $\boldsymbol{n}_\perp = \boldsymbol{n} - \boldsymbol{n}_\parallel = \boldsymbol{n} - \boldsymbol{v}_2 n_\parallel/v_2$, and omitting the component parallel to $\boldsymbol{n}$ [which does not contribute to the vector product with $\boldsymbol{n}$ present in Eq. (46)], brings the azimuthally averaged radiation amplitude to the form

$$\boldsymbol{n}\times\langle\boldsymbol{J}\rangle_{\mathrm{azim}\,\boldsymbol{v}_\perp} = \frac{\boldsymbol{n}\times\boldsymbol{v}_2}{v_2}2\gamma^2 G(\Sigma, X), \tag{50}$$

with

$$2\gamma^2 G = \frac{1}{1 - n_\parallel v_2/c} - \frac{1}{n_\perp^2}\left(n_\parallel c - \frac{n_\parallel - v_\parallel}{\sqrt{(c - n_\parallel v_\parallel)^2 - n_\perp^2 v_\perp^2}}\right).$$

In the small-angle approximation, $n_\perp = \theta \ll 1$, $v_\perp/c = \chi \ll 1$, $n_\parallel = 1 - \theta^2/2$, $v_\parallel/c = 1 - (\gamma^{-2} + \chi^2)/2$, factor G becomes

$$\begin{aligned}G &\approx \frac{1}{1+\gamma^2\theta^2} \\ &\quad - \frac{1}{2\gamma^2\theta^2}\left(1 + \frac{\theta^2 - \chi^2 - \gamma^{-2}}{\sqrt{[\gamma^{-2} + (\theta-\chi)^2][\gamma^{-2} + (\theta+\chi)^2]}}\right) \\ &\equiv \frac{1}{1+\Theta^2} - \frac{1}{2\Theta^2}\left(1 + \frac{\Theta^2 - X - 1}{\sqrt{(X + 1 - \Theta^2)^2 + 4\Theta^2}}\right),\end{aligned} \tag{51}$$

with $X = \gamma^2\chi^2$. Function (51) is everywhere positive and bounded ($0 < G < 1$), and monotonously decreases with the increase of Θ or decrease of X [see Fig. 2(a)].

In the following, we will need to know various asymptotic limits of function G. At small Θ, it expands as

$$\begin{aligned}G &= \sum_{n=0}^{\infty}\Theta^{2n}\left\{(-1)^n\right. \\ &\quad \left. + \frac{1}{2(X+1)^{n+1}}\left[P_{n+1}\left(\frac{X-1}{X+1}\right) - P_n\left(\frac{X-1}{X+1}\right)\right]\right\} \\ &\underset{\Theta\ll 1}{\simeq} 1 - \frac{1}{(1+X)^2} + \mathcal{O}(\Theta^2),\end{aligned} \tag{52}$$

[6]More elaborate empirical formulas exist accounting also for Z dependence of the prelogarithmic factor [32], but to keep the treatment simple, and expose numerical differences between the approaches, we will confine ourselves here to parametrization (45).

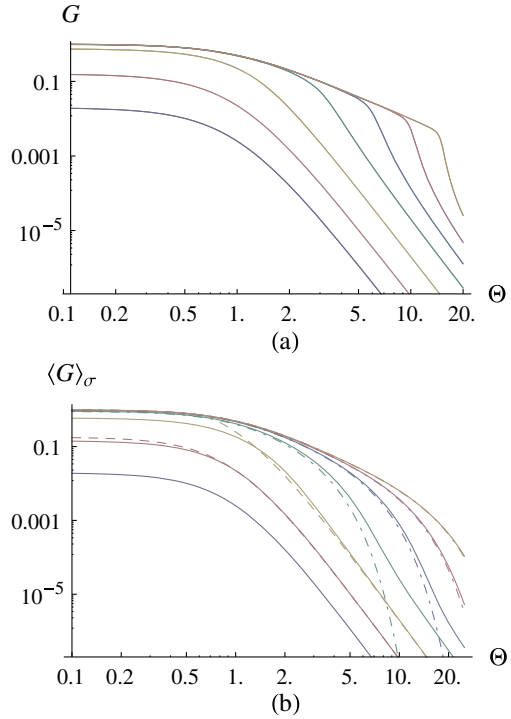

FIG. 2 (color online). (a) LogLog plot of the azimuthally averaged electromagnetic current at one scattering, Eq. (51), for scattering angles $\gamma\chi = 0.1, 0.3, 1, 3, 6, 10, 15$ (solid curves, bottom to top). (b) The same for the Gaussian-weighted azimuthally averaged electromagnetic current at one scattering, Eq. (62b). Dashed curves, approximation (63b). Dot-dashed curves, approximation (64).

where P_n are Legendre polynomials [33] arising as coefficients in the expansion $(1-2\zeta h+h^2)^{-1/2} = \sum_{n=0}^{\infty} P_n(\zeta)h^n$.

Also, at small X,

$$G = \frac{1}{2\Theta^2}\sum_{n=0}^{\infty}\frac{X^{n+1}}{(\Theta^2+1)^{n+1}}\left[P_n\left(\frac{\Theta^2-1}{\Theta^2+1}\right) - \frac{\Theta^2-1}{\Theta^2+1}P_{n+1}\left(\frac{\Theta^2-1}{\Theta^2+1}\right)\right] \tag{53a}$$

$$\underset{X\ll 1}{\simeq}\frac{2}{(1+\Theta^2)^3}X + \mathcal{O}(X^2). \tag{53b}$$

Here the leading term is proportional to $X \propto \chi^2$, whereas in the dipole approximation the current is $\propto\chi$ but vanishes after azimuthal averaging [see Eq. (8)]. Thus, the leading term (53b) corresponds to a "quadrupole" approximation.

On the other hand, at large χ and fixed θ,

$$G \underset{X\gg 1}{\approx}\begin{cases}\frac{1}{1+\Theta^2} & (\theta<\chi)\\ 0 & (\theta>\chi)\end{cases}. \tag{54}$$

Factor $\frac{1}{1+\Theta^2}$ here describes the radiation from the $\boldsymbol{v}_2$ half line alone. As for the radiation from the $\boldsymbol{v}$ end, it is smeared by the azimuthal averaging, but in any case, the interjet region extends only out to the polar angle $\theta\approx\chi$. It is remarkable that function G features no enhancement around $\theta=\chi$, in spite of the existence of the $\boldsymbol{v}$ jet. So, after the azimuthal averaging, the latter jet does not manifest itself as a peak in the angular distribution of radiation. For $\theta>\chi$, the radiation is suppressed much more strongly because radiation amplitudes from $\boldsymbol{v}_2$ and $\boldsymbol{v}$ lines nearly cancel.

B. The aggregate spectrum

Employing representation Eq. (50) in Eq. (46) ultimately leads to

$$(\boldsymbol{n}\times\langle\boldsymbol{J}_{21}\rangle)\cdot(\boldsymbol{n}\times\langle\boldsymbol{J}_{32}\rangle) = -4\gamma^4\theta^2\langle G\rangle_1\langle G\rangle_2, \tag{55}$$

where

$$\langle G\rangle_i = \int_0^\infty d\chi^2\frac{dw_i}{d\chi^2}G(\chi,\theta), \tag{56}$$

and we invoked the identity $(\boldsymbol{n}\times\boldsymbol{v}_2/v_2)^2=\theta^2$. The minus sign in Eq. (55), i.e., the destructive interference between the currents, retraces to the general property of saturation of radiation in the nondipole regime. In Eq. (3b), though, factor (55) is yet multiplied by an ω-dependent factor $\cos\Phi$, and the corresponding product is to be integrated over polar radiation angles. Since $\cos\Phi$ is sign-alternating, the spectrum may oscillate with the increase of Ω, not just experience a suppression. Combining with the previously computed bremsstrahlung contributions from individual plates, which are ω independent, we get

$$\left\langle\frac{dI}{d\omega}\right\rangle = \frac{2e^2}{\pi c}\left[\langle F\rangle_1+\langle F\rangle_2 - \int_0^\infty d\Theta^2\Theta^2\langle G\rangle_1\langle G\rangle_2\cos\Omega(1+\Theta^2)\right]. \tag{57}$$

The dependence of function (57) on Ω is shown in Fig. 3, and it evidently exhibits an oscillatory behavior.

To determine the magnitude and the phase of the oscillations, note that at $\Omega\gg 1$, the integral in the last term of (57) is dominated by the vicinity of the lower end point, and its evaluation with $\langle G\rangle_{1,2}(\Theta) = \langle G\rangle_{1,2}(0) + \mathcal{O}(\Theta^2)$ yields the asymptotics

$$\left\langle\frac{dI}{d\omega}\right\rangle \underset{\Omega\to\infty}{\simeq}\frac{2e^2}{\pi c}\left[\langle F\rangle_1+\langle F\rangle_2 + \frac{\cos\Omega}{\Omega^2}\langle G\rangle_1(0)\langle G\rangle_2(0) + \mathcal{O}(\Omega^{-3})\right]. \tag{58}$$

According to this result, maxima of $dI/d\omega$ appear at

$$\Omega\approx 2\pi n, \tag{59}$$

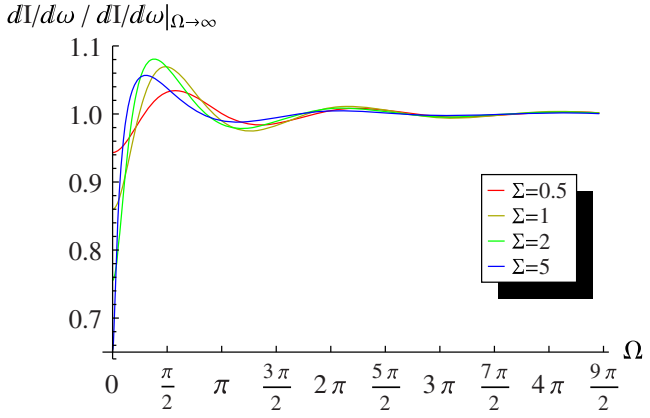

FIG. 3 (color online). Oscillations of spectrum of the bremsstrahlung on two foils, computed for Gaussian scattering-angle distribution functions with rms $\Sigma_1 = \Sigma_2 = 0.5$ (thin red curve), 1 (yellow), 2 (green), 5 (blue). At $\Omega \gtrsim \frac{t_{21}}{\max\{l_1,l_2\}}$, the spectrum must rise again, and reach the Bethe-Heitler constant value (see Sec. VI).

with integer n, independently of shapes of distribution functions $\langle G\rangle_{1,2}$. That simple prediction is confirmed by Fig. 3. A geometrical interpretation for the rule (59) in the spirit of wave optics is that interference maxima occur whenever the distance between the foils equals to an integer number of full coherence lengths $2\pi l_f$.

Concerning the principal maximum, however, the situation is less trivial, and there is no possibility to associate it with the case of a unit wavelength shift as proposed in [14]. For $\Omega \lesssim 1$, formula (58) is clearly inapplicable, but from the viewpoint of exact formula (57), the principal maximum of $dI/d\omega$ emerges when in the integrand of the last term, the maximum of the product[7] $\Theta^2\langle G\rangle_1(\Theta)\langle G\rangle_2(\Theta)$, achieved at some $\Theta = \Theta_\star(\Sigma)$, coincides with the extremum of the other factor $\cos\Omega(1+\Theta^2)$:

$$\Omega_\star = \frac{\pi}{1+\Theta_\star^2}, \tag{60}$$

where $\cos\Omega(1+\Theta^2) = -1$. That situation has to be distinguished from the case $\Omega = \pi$ in Eq. (58), where the existence of a maximum for $\Theta^2\langle G\rangle_1\langle G\rangle_2$ was of little consequence as long as there were several oscillations of $\cos\Omega(1+\Theta^2)$ within its width, and the region of dominant contribution shifted to the end point $\Theta = 0$. In the latter case, the half-wavelength shift corresponded to a spectral *minimum* next to the principal maximum. As opposed to that, case (60) with the account of the denominator $1+\Theta_\star^2$ can be called the inclined half-wavelength, which is numerically close to quarter-wavelength.

It is worth stressing in this regard that although the denominator in relation (60) depends on Σ, that dependence is not dramatic, since for any Σ, $\Theta_\star(\Sigma) \sim 1$. This is clear, insofar as even at large Σ, the contributing Θ's in Eq. (57) are $\Theta \sim 1$, i.e., $\theta \sim \gamma^{-1}$ with respect to the direction $\boldsymbol{v}_2$. Therefore, the use of the in-medium coherence length [34]

$$l_c(\omega,\Sigma) = \frac{l_f(\omega)}{1+\Sigma^2} \tag{61}$$

in the resonance condition $ct_{21} \propto l_c(\omega,\Sigma)$ is *unjustified*. In fact, the usage of (61) in application to the present problem led in [16] to an appreciable underestimate of the location of the first spectral maximum.

Finally, an important feature is the spectral *minimum* at $\omega = 0$, i.e., at zero wavelength shift. That limit corresponds to a situation when the radiation amplitude completely factorizes from the scattering one, wherewith the radiation on two plates equals to that on one plate with the aggregate thickness. Such a relation is not obvious from Eq. (57), but can be checked by straightforward integration over Θ after setting $\cos\Omega(1+\Theta^2) \to 1$; we will also provide its simpler derivation in Sec. V A. The spectral dip at $\omega \to 0$ also resembles the corresponding feature in the LPM spectrum, with the difference that our spectrum in this limit does *not* go to zero. That reflects finite target thickness effects, which are absent in the LPM theory. Increasing the number of scattering plates would ultimately lower the ratio $dI/d\omega/dI/d\omega|_{\Omega\to\infty}$ to zero, but for two plates, it cannot fall below $1/2$.

C. Weighting with Gaussian distribution

To deduce now the consequences from the averaging over scattering angles, let us first assume $\frac{dw}{d^2\chi}$ in (56) to be a Gaussian weighting distribution (16). The averaging of G with this distribution simplifies after an integration by parts:

$$\langle G\rangle_\sigma(\Theta) = \int_0^\infty d\chi^2 \frac{1}{\sigma^2} e^{-\chi^2/\sigma^2} G$$

$$\equiv \int_0^\infty d\chi^2 e^{-\chi^2/\sigma^2} \frac{\partial}{\partial\chi^2} G \tag{62a}$$

$$= \int_0^\infty dX \frac{2e^{-X/\Sigma^2}}{[(X+1-\Theta^2)^2+4\Theta^2]^{3/2}}. \tag{62b}$$

The behavior of function (62b) is illustrated in Fig. 2(b) for several values of Σ. It is basically similar to that of G shown in Fig. 2(a), but is smoother at $\Theta \sim \Sigma \gg 1$, the latter property being expectable as long as the sharp drop in function (54) at $\theta \approx \chi$ is smeared out by the averaging over χ.

Numerically, Eq. (57) with entries (22), (62b) proves to be equivalent to Eqs. (2.34), (2.36) of [16] under the correspondence rule (32), although analytically, the proof of equivalence of both approaches is nontrivial. Our representation is advantageous for the analytic study of Σ and Ω dependences. Let us derive with its aid small- and

[7]The existence of a maximum for this expression at nonzero Θ owes in particular to the factor Θ^2, which is due to the cancellation of interference effects at small Θ.

large-Σ asymptotics of function $\langle G\rangle_\sigma$, which will be needed in what follows.

At small Σ, plugging expansion (53a) into Eq. (62a), and integrating termwise, we obtain

$$\langle G\rangle_\sigma(\Theta) = \frac{1}{2\Theta^2}\sum_{n=0}^{\infty}\frac{(n+1)!\Sigma^{2(n+1)}}{(\Theta^2+1)^{n+1}}\left[P_n\left(\frac{\Theta^2-1}{\Theta^2+1}\right) - \frac{\Theta^2-1}{\Theta^2+1}P_{n+1}\left(\frac{\Theta^2-1}{\Theta^2+1}\right)\right] \tag{63a}$$

$$\underset{\Sigma\ll 1}{\simeq} 2\Sigma^2(1+\Theta^2)^{-3} + \mathcal{O}(\Sigma^4). \tag{63b}$$

Similarly to Eq. (19), expansion (63a) diverges, but again, it remains sensible as an asymptotic series. Its leading term (63b) coincides with the asymptotics of the nonaveraged expression (53b), granted that there the χ dependence factorizes. The behavior of approximation (63b) is shown in Fig. 2(b) by dashed curves.

On the other hand, at significant Σ, it is legitimate to expand e^{-X/Σ^2} to Taylor series about point $X=\Theta^2-1$ and integrate termwise:

$$\begin{aligned}\langle G\rangle_\sigma(\Theta) &\underset{\Sigma\gg 1}{\approx} e^{-\frac{\Theta^2-1}{\Sigma^2}}\int_0^\infty dX\frac{2}{[(X+1-\Theta^2)^2+4\Theta^2]^{3/2}}\times\left(1+\frac{\Theta^2-1-X}{\Sigma^2}\right)\\ &= \frac{1}{1+\Theta^2}e^{-\frac{\Theta^2-1}{\Sigma^2}}\left(1-\frac{2}{\Sigma^2}\right)\\ &\approx \frac{1}{1+\Theta^2}e^{-\frac{1+\Theta^2}{\Sigma^2}}.\end{aligned} \tag{64}$$

According to Fig. 2(b) (dot-dashed curves), approximation (64) works well for $\Sigma>3$. At large Σ and fixed Θ, the exponential here tends to unity, retrieving the form (54).

D. Averaging with Molière distribution: Impact parameter representation

If instead of a Gaussian we wish to use a more rigorous Molière weighting distribution (33), it is more convenient to return to representation (3b) for the radiation spectrum. In the last line of Eq. (3b), the product of currents consists of four terms, which have similar structure. It thus suffices to calculate only one of them:

$$O_{13} = \int d^2n\frac{\boldsymbol{n}-\boldsymbol{v}_1/c}{\gamma^{-2}+(\boldsymbol{n}-\boldsymbol{v}_1/c)^2}\cdot\frac{\boldsymbol{n}-\boldsymbol{v}_3/c}{\gamma^{-2}+(\boldsymbol{n}-\boldsymbol{v}_3/c)^2}\times\cos\frac{\omega t_{21}}{2}[\gamma^{-2}+(\boldsymbol{n}-\boldsymbol{v}_2/c)^2], \tag{65}$$

the others being reconstructable by replacements $\boldsymbol{v}_3\to\boldsymbol{v}_2$ or/and $\boldsymbol{v}_1\to\boldsymbol{v}_2$.

Changing here the integration variable to $\boldsymbol{n}'_\perp=\boldsymbol{n}-\boldsymbol{v}_2/c$ and inserting representations (35) for the first factor in the first line of (65), and a complex conjugate representation for the second factor, one brings O_{13} to the form of an integral over impact parameters:

$$O_{13} = \int d^2\xi_1 e^{i(\boldsymbol{v}_2-\boldsymbol{v}_1)\cdot\boldsymbol{\xi}_1}\frac{\partial}{\partial\boldsymbol{\xi}_1}K_0(\xi_1/\gamma)\cdot\int d^2\xi_3 e^{i(\boldsymbol{v}_3-\boldsymbol{v}_2)\cdot\boldsymbol{\xi}_3}\frac{\partial}{\partial\boldsymbol{\xi}_3}K_0(\xi_3/\gamma)\mathfrak{Re}S_\omega(\boldsymbol{\xi}_1-\boldsymbol{\xi}_3,t_{21}), \tag{66}$$

where

$$S_\omega(\boldsymbol{\xi}_1-\boldsymbol{\xi}_3,t_{21}) = \frac{1}{(2\pi)^2}\int d^2n'_\perp e^{i\boldsymbol{n}'_\perp\cdot(\boldsymbol{\xi}_1-\boldsymbol{\xi}_3)-i\frac{\omega t_{21}}{2}(\gamma^{-2}+\boldsymbol{n}'^2_\perp)}. \tag{67}$$

The latter function for $t_{21}>0$ may be regarded as a Green's function for the two-dimensional free Schrödinger equation on the light front:

$$\left[-i\frac{\partial}{\partial t_{21}}+\frac{\omega}{2}\left(\gamma^{-2}-\frac{\partial^2}{\partial(\boldsymbol{\xi}_1-\boldsymbol{\xi}_3)^2}\right)\right]S_\omega(\boldsymbol{\xi}_1-\boldsymbol{\xi}_3,t_{21})\vartheta(t_{21}) = -i\delta(\boldsymbol{\xi}_1-\boldsymbol{\xi}_3)\delta(t_{21}) \tag{68}$$

[in the lhs, $\vartheta(t_{21})$ being the Heaviside unit step function], and evaluates in closed form:

$$\mathfrak{Re}S_\omega(\boldsymbol{\xi}_1-\boldsymbol{\xi}_3,t_{21}) = \frac{1}{2\pi\omega t_{21}}\sin\left[\frac{(\boldsymbol{\xi}_1-\boldsymbol{\xi}_3)^2}{2\omega t_{21}}-\frac{\omega t_{21}}{2\gamma^2}\right]. \tag{69}$$

Note that it depends only on the difference between $\boldsymbol{\xi}_1$ and $\boldsymbol{\xi}_3$, just as in Eq. (57) the cosine depends, besides ωt_{21}, only on the angle between $\boldsymbol{v}_2$ and $\boldsymbol{n}$.

Restoring the rest of the interference terms by substitutions $\boldsymbol{v}_1\to\boldsymbol{v}_2$ or $\boldsymbol{v}_3\to\boldsymbol{v}_2$, and combining them, we get

$$\frac{dI}{d\omega} = \frac{dI_1}{d\omega}+\frac{dI_2}{d\omega} + \frac{2e^2}{\pi^2 c}\int d^2\xi_1 d^2\xi_3(1-e^{i(\boldsymbol{v}_1-\boldsymbol{v}_2)\cdot\boldsymbol{\xi}_1/c})(1-e^{i(\boldsymbol{v}_2-\boldsymbol{v}_3)\cdot\boldsymbol{\xi}_3/c})\times\frac{\partial}{\partial\boldsymbol{\xi}_1}K_0(\xi_1/\gamma)\cdot\frac{\partial}{\partial\boldsymbol{\xi}_3}K_0(\xi_3/\gamma)\mathfrak{Re}S_\omega(\boldsymbol{\xi}_1-\boldsymbol{\xi}_3,t_{21}). \tag{70}$$

Convolving this with the Molière distribution function (33), and integrating over azimuths of $\boldsymbol{\xi}_1$ and $\boldsymbol{\xi}_3$, leads to the result

$$\left\langle \frac{dI}{d\omega} \right\rangle_{\rm M} = \left\langle \frac{dI_1}{d\omega} \right\rangle_{\rm M} + \left\langle \frac{dI_2}{d\omega} \right\rangle_{\rm M} + \frac{2e^2}{\pi c\Omega} \int_0^\infty d\rho_1 \rho_1 K_1(\rho_1) \{1 - e^{-n_1 l_1 \int d\sigma(\chi)[1-J_0(\rho_1\gamma\chi)]}\}$$
$$\times \int_0^\infty d\rho_3 \rho_3 K_1(\rho_3) \{1 - e^{-n_2 l_2 \int d\sigma(\chi)[1-J_0(\rho_3\gamma\chi)]}\} \cos\left(\frac{\rho_1^2+\rho_3^2}{4\Omega} - \Omega\right) J_1\left(\frac{\rho_1\rho_3}{2\Omega}\right), \tag{71}$$

where $\rho_{1,3} = \xi_{1,3}/\gamma$. Note that after the integration over the azimuths, the dependence of the Green function only on the impact parameter vector difference is somewhat disguised.

At large Ω, upon approximations $\cos(\frac{\rho_1^2+\rho_3^2}{4\Omega} - \Omega) \to \cos\Omega$, $J_1(\frac{\rho_1\rho_3}{2\Omega}) \to \frac{\rho_1\rho_3}{4\Omega}$, the double integral in Eq. (71) factorizes:

$$\left\langle \frac{dI}{d\omega} \right\rangle_{\rm M} \underset{\Omega\to\infty}{\to} \left\langle \frac{dI_1}{d\omega} \right\rangle_{\rm M} + \left\langle \frac{dI_2}{d\omega} \right\rangle_{\rm M} + \frac{e^2\cos\Omega}{2\pi c\Omega^2} \int_0^\infty d\rho_1 \rho_1^2 K_1(\rho_1) \{1 - e^{-n_1 l_1 \int d\sigma(\chi)[1-J_0(\rho_1\gamma\chi)]}\}$$
$$\times \int_0^\infty d\rho_3 \rho_3^2 K_1(\rho_3) \{1 - e^{-n_2 l_2 \int d\sigma(\chi)[1-J_0(\rho_3\gamma\chi)]}\}. \tag{72}$$

This form proves to be equivalent to Eq. (58), by virtue of the identity

$$\frac{1}{2}\int_0^\infty d\rho\rho^2 K_1(\rho)\{1 - e^{-nl\int d\sigma(\chi)[1-J_0(\rho\gamma\chi)]}\} \tag{73a}$$
$$\equiv \frac{1}{2}\int d^2\chi \frac{dw_{\rm M}}{d^2\chi} \int_0^\infty d\rho\rho^2 K_1(\rho)[1 - J_0(\rho\gamma\chi)]$$
$$= \int d^2\chi \frac{dw_{\rm M}}{d^2\chi}\left[1 - \frac{1}{(1+X)^2}\right] = \langle G\rangle_{\rm M}(0), \tag{73b}$$

where in the last line we used Eq. (52).

V. ANALYSIS OF THE INTERFERENCE PATTERN

The spectrum of radiation on two foils evaluated in the previous section is a function of three variables: Σ_1, Σ_2, and Ω, the dependences on which are intertwined. In the limiting cases, though, it reduces to simpler functions as demonstrated below.

A. Visibility of the low-ω dip

For the experimental practice, it is often desirable to estimate visibilities of gross features of the spectrum and optimize them by choosing appropriate foil materials and their thicknesses. The interference term reaches its largest absolute value at $\omega = 0$. Therefore, it is natural to consider the characteristic quantity

$$V_0(\Sigma_1,\Sigma_2) = 1 - \left\langle \frac{dI}{d\omega} \right\rangle\Big|_{\omega=0} \Big/ \left\langle \frac{dI}{d\omega} \right\rangle\Big|_{\omega=\infty}, \tag{74}$$

which may be called the low-ω dip visibility. With the aid of Eq. (57), it can be explicitly written as

$$V_0 = \frac{\int_0^\infty d\Theta^2\Theta^2 \langle G\rangle_1(\Theta)\langle G\rangle_2(\Theta)}{\langle F\rangle_1 + \langle F\rangle_2}. \tag{75a}$$

As we already mentioned at the end of Sec. IV B, in the soft photon limit the spectrum must reduce to a spectrum from a single foil of aggregate thickness. This can now be easily verified based on the impact parameter representation (71) (before integrations over the azimuths of impact parameters). There, $S_\omega \underset{\Omega\to 0}{\to} \delta(\boldsymbol{\xi}_1 - \boldsymbol{\xi}_3)$, and terms $\frac{dI_1}{d\omega}$, $\frac{dI_2}{d\omega}$ cancel with some of the interference terms, leaving $\frac{dI}{d\omega} \underset{\Omega\to 0}{\to} \frac{dI_1(l_1+l_2)}{d\omega}$. Thereby, V_0 indeed reduces to

$$V_0 = 1 - \frac{\langle F\rangle_{l_1+l_2}}{\langle F\rangle_1 + \langle F\rangle_2}. \tag{75b}$$

At small Σ, from Eqs. (75b) and (21) we find

$$V_0 \underset{\Sigma_{1,2}\ll 1}{\simeq} \frac{3}{5}\frac{1}{\Sigma_1^{-2} + \Sigma_2^{-2}}; \tag{76}$$

i.e., essentially it is proportional to the smallest among Σ_1^2, Σ_2^2.

At large Σ_1, Σ_2, from Eqs. (75b) and (23),

$$V_0 \underset{\Sigma_{1,2}\gg 1}{\simeq} \frac{1}{2} - \frac{\ln(\Sigma_1/\Sigma_2 + \Sigma_2/\Sigma_1)}{2(\ln\Sigma_1\Sigma_2 - \gamma_{\rm E} - 1)}. \tag{77}$$

Thus, in principle, asymptotically V_0 tends to 1/2. That is natural: because radiation at one plate saturates as a function of its thickness, the radiation at any two strongly scattering foils must be about twice stronger than on one of them. But practically, such a saturation is achieved only logarithmically, and too remotely, so the second term in Eq. (77) is usually important.

The behavior of function (75) and its asymptotic approximation (77) is illustrated in Fig. 4(b) by black solid and dashed curves. For comparison, the purple dot-dashed curve also shows the prediction of Blankenbecler's theory, namely, when in Eq. (75b) $\langle F\rangle_\sigma$ is replaced by $F(\Sigma/2)$. Notably, that curve intersects with the exact result at $\Sigma \approx 3$ and keeps close to it at greater Σ. But at $\Sigma \sim 1$ the difference is relatively large. It may be interesting to note that the Blankenbecler-Drell prediction for V_0 is lower than the exact one; i.e., the neglect of fluctuations leads to an underestimation of the interference effect in radiation. That means that under the conditions of cancellation of dipole contributions in the interference, fluctuations help create uncompensated contributions.

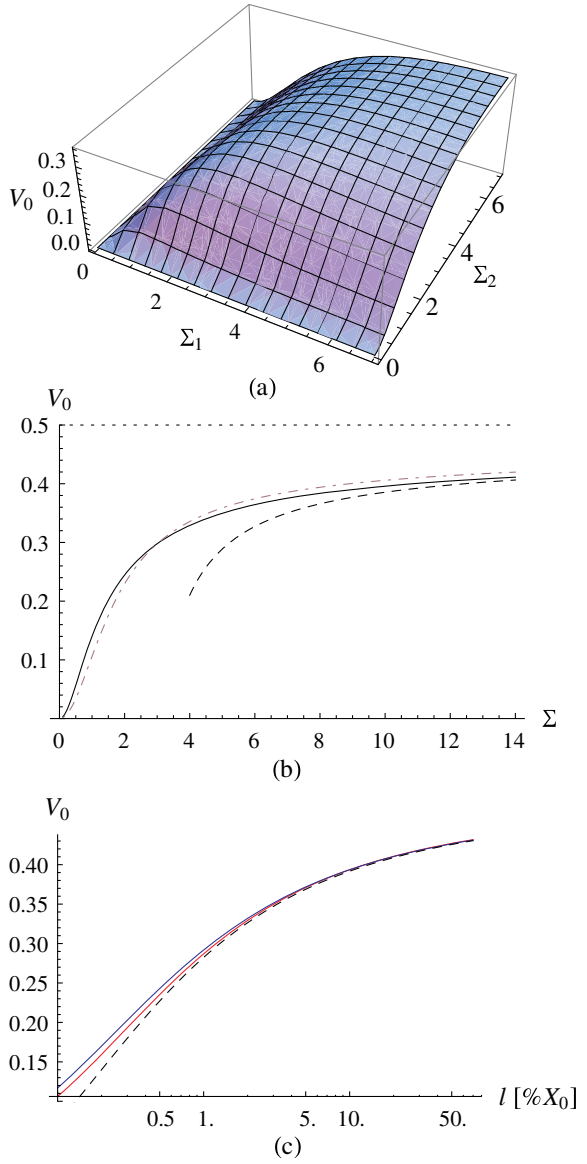

FIG. 4 (color online). The visibility of the low-ω dip, Eq. (75b). (a) For Gaussian averaging and arbitrary Σ_1, Σ_2. (b) For Gaussian averaging and $\Sigma_1 = \Sigma_2 = \Sigma$. Solid black curve, exact expression (75). Dashed black curve, its asymptotics (77). Purple dot-dashed curve, the visibility in the Blankenbecler-Drell approximation $\langle F\rangle_\sigma \to F(\Sigma/2)$. (c) For Molière averaging. Blue curve, carbon; red curve, gold; black dashed curve, Gaussian averaging with rms scattering angle computed by formula (45).

It is also useful to compare in this limit the predictions of Gaussian and Molière averaging. From Fig. 4(c), it follows that the Gaussian averaging prediction becomes inaccurate at $l \lesssim 10^{-3}X_0$, just where the accuracy of approximation (45) itself drops below 10%.

B. Visibility of secondary minima and maxima

In the opposite limit of large ω, according to Eq. (58), the interference visibility may be characterized by the ratio

$$V_\infty(\Sigma_1,\Sigma_2) = \frac{\langle G\rangle_1(0)\langle G\rangle_2(0)}{\langle F\rangle_1 + \langle F\rangle_2}. \tag{78}$$

At small Σ, this quantity behaves as

$$V_\infty \underset{\Sigma_{1,2}\ll 1}{\simeq} \frac{12}{\Sigma_1^{-2}+\Sigma_2^{-2}}, \tag{79}$$

while at large Σ_1, Σ_2, it decreases logarithmically:

$$V_\infty \underset{\Sigma_{1,2}\gg 1}{\simeq} \frac{1}{2(\ln\Sigma_1\Sigma_2 - \gamma_E - 1)}. \tag{80}$$

The dependence of V_∞ on both parameters Σ_1 and Σ_2 is portrayed in Fig. 5(a). Its maximum is achieved at $\Sigma_1 = \Sigma_2 \approx 1$ [see Fig. 5(b)]. There, the function still does not exceed 0.7. Yet, one remembers that in (58) it is multiplied

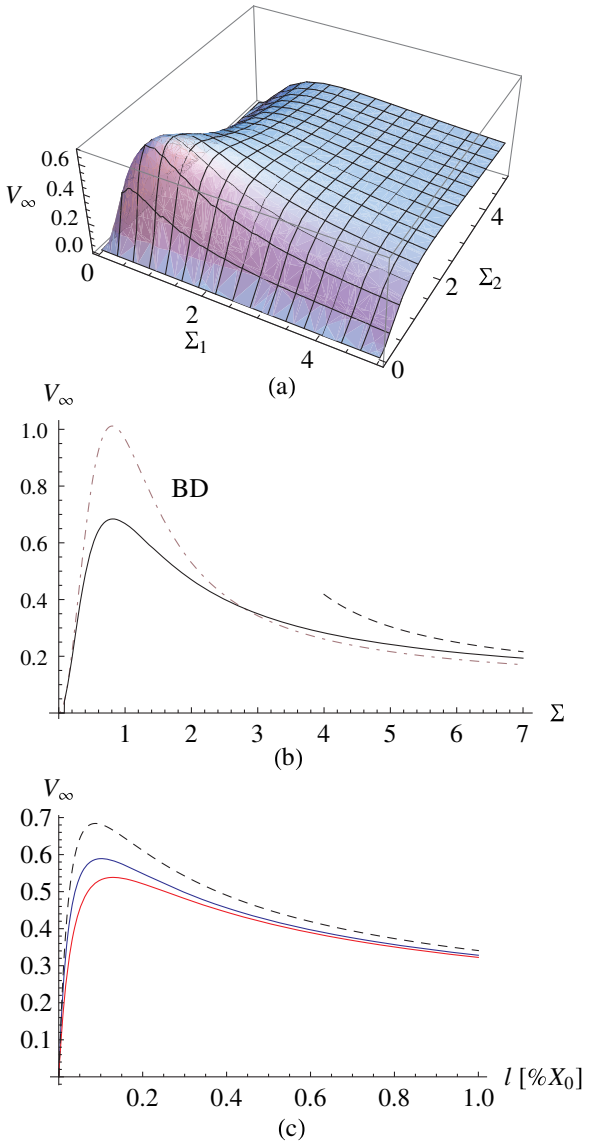

FIG. 5 (color online). Same as Fig. 4, for the visibility of secondary minima and maxima, Eq. (78). The dashed curve in (b) obeys Eq. (80) for $\Sigma_1 = \Sigma_2 = \Sigma$.

by Ω^{-2} with $\Omega \gtrsim \pi$; hence, the actual visibility in the high-ω region is on the level of a few percent, demanding substantial measurement statistics.

For comparison, Fig. 5(b) by the dot-dashed curve shows the behavior of Eq. (78) after replacement of averaged radiation form factors by nonaveraged functions of averaged argument:

$$\langle F\rangle_\sigma \to F(\Sigma/2), \qquad \langle G\rangle_\sigma(0) \to G(\Sigma,0) = 1 - \frac{1}{(1+\Sigma^2)^2} \quad \text{(LP-BD)}, \tag{81}$$

which we presume to correspond to the Blankenbecler-Drell approximation. It intersects with the exact result at $\Sigma \approx 2.5$ and keeps close to it at greater Σ, but at $\Sigma \approx 1$ the difference is rather large.

Figure 5(c) compares predictions of Eq. (78) when averaging is carried out with Molière distribution, by Eqs. (73a), (43) (the blue solid curve for carbon, the red solid curve for gold), and with Gaussian distribution, Eqs. (62b) and (22) (black dashed curve). There is a distinct difference between the predictions around the maximum, which is achieved at $l \approx 10^{-3}X_0$, i.e., $\Sigma \approx 1$. The sign of this difference means that in the region of substantial photon energies, the account of fluctuations of scattering leads to a lowering of the interference effect in radiation, contrary to the situation with V_0 in the previous subsection. That can be explained by recalling that fluctuations always tend to suppress the radiation, but at $\omega = 0$, where the interference effect itself is suppressive, that worked towards increasing the effect, whereas in the large-ω region it just lowers both amplitudes $\langle G\rangle_1(0)$ and $\langle G\rangle_2(0)$ in the interference term.

C. Spectrum oscillation shapes

For a generic case, integral (57) has to be evaluated numerically. But for limiting cases (53b) and (54), the integration can be done analytically. For completeness, in the remainder of this section, we will quote the corresponding formulas for the limiting spectral shapes, and compare them with results of [16], obtained for the same limits and at $\sigma_1 = \sigma_2$.

1. Small-angle scattering in both plates

To begin with, consider the case when scattering angles in both foils are small. Inserting (63b) into (57), we find

$$\left\langle \frac{dI}{d\omega}\right\rangle \underset{\Sigma_{1,2}\ll 1}{\simeq} \left(\left\langle \frac{dI_1}{d\omega}\right\rangle + \left\langle \frac{dI_2}{d\omega}\right\rangle\right)\left[1 + \frac{3}{5}\frac{1}{\Sigma_1^{-2}+\Sigma_2^{-2}} g_{\rm qq}(\Omega)\right], \tag{82}$$

where

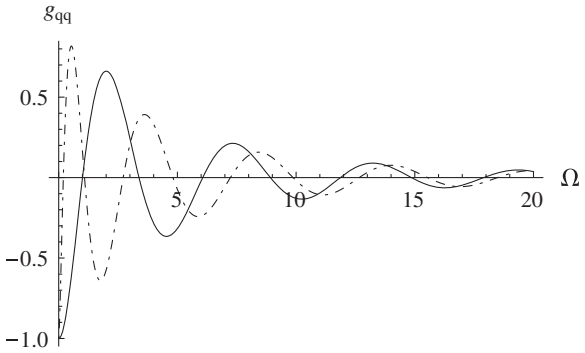

FIG. 6. Interference function for the case of double small-angle scattering. Solid curve, Eq. (84)—close to the red curve of Fig. (3). Blue dot-dashed curve, Baier-Katkov's function $\frac{10}{3}G(\Omega)$ [16].

$$\left\langle \frac{dI_1}{d\omega}\right\rangle \underset{\Sigma_1\ll 1}{\simeq} \frac{2e^2}{3\pi c}\Sigma_1^2\left(1 - \frac{3}{10}\Sigma_1^2\right), \tag{83}$$

and

$$g_{\rm qq}(\Omega) = -20\int_0^\infty \frac{d\Theta^2\Theta^2}{(1+\Theta^2)^6}\cos\Omega(1+\Theta^2), \tag{84}$$

is the quadrupole-quadrupole interference function, normalized by condition $g_{\rm qq}(0) = -1$. The latter function achieves its first maximum at $\Omega \approx 2$ (see Fig. 6). According to Eqs. (82), (84) for small Σ_1, Σ_2, the visibility of spectral fringes is $\sim\frac{3}{5}\min\{\Sigma_1^2, \Sigma_2^2\}$.

It should be noted that our function (84) appears to differ from function $\frac{10}{3}G(T)$ obtained in [16], Eq. (2.37). The comparison of those functions in Fig. 6 shows marked differences, except in the extremes $\Omega = 0$ and $\Omega \to \infty$. We believe therefore that the corresponding limiting result of [16] is in error, although it was derived from correct generic Eqs. (2.34), (2.36) of [16].[8]

2. Radiation at double large-angle scattering

An opposite limiting case is when scattering angles on each of the foils are $\gg \gamma^{-1}$. Inserting Eq. (64) into (57), one obtains

$$\left\langle \frac{dI}{d\omega}\right\rangle \underset{\Sigma_{1,2}\gg 1}{\simeq} \frac{2e^2}{\pi c}[\ln\Sigma_1^2 + \ln\Sigma_2^2 - 2\gamma_{\rm E} - 2 + g_{\rm ll}(\Sigma_1^{-2}+\Sigma_2^{-2}, \Omega)], \tag{85}$$

where

[8]In order to derive the corresponding result from Eqs. (2.34), (2.36) of [16], one has to expand them up to order $\sim b^{-2}$ [while contributions $\sim b^{-1}$ from $2dw^{(2)}_{br1}/d\omega$ and $dw^{(2)}_{br3}/d\omega$ must cancel], which is a rather tedious procedure.

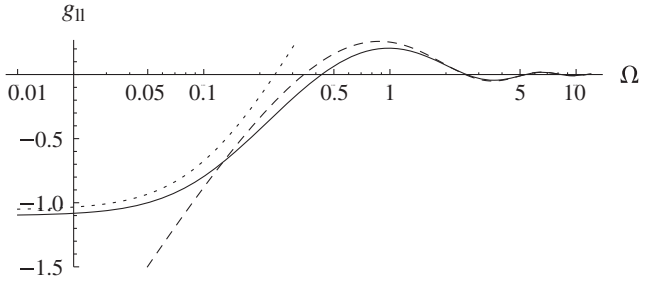

FIG. 7. Interference function for the case of double large-angle scattering ($\Sigma_1^{-2}+\Sigma_2^{-2}=0.1$). Solid curve, Eq. (86)—close to the blue curve of Fig. 3. Dashed curve, $g_{\rm II}(0,\Omega)$. Dotted curve, asymptotics (87).

$$g_{\rm II}(\xi,\Omega)=-\Re\mathrm{e}\left[\int_0^\infty \frac{d\Theta^2\Theta^2}{(1+\Theta^2)^2}e^{-(1+\Theta^2)(\xi+i\Omega)}\right] =e^{-\xi}\cos\Omega-\Re\mathrm{e}[(1+\xi+i\Omega)E_1(\xi+i\Omega)], \tag{86}$$

with $E_1(z)=\int_1^\infty dt\frac{e^{-zt}}{t}$ the exponential integral. Term $\xi=\Sigma_1^{-2}+\Sigma_2^{-2}$ in the argument of E_1 is negligible if $\Omega\gg\Sigma_1^{-2}+\Sigma_2^{-2}\ll 1$; thereat our Eq. (85) reduces to Eq. (2.45) of [16]. This limiting function achieves its main maximum at $\Omega\approx 0.9$ (see Fig. 7), which agrees with the conclusions of Blankenbecler-Drell and Baier-Katkov that the maximum is achieved at $\Omega\approx 1$.[9] However, for small Ω, term ξ in the argument of E_1 is crucial. There, $E_1(z)\simeq -\ln z-\gamma_{\rm E}$, wherewith

$$g_{\rm II}(\xi,\Omega)\underset{\xi\ll 1}{\approx}\frac{1+\xi}{2}\ln(\xi^2+\Omega^2)+\gamma_{\rm E}+1-\xi. \tag{87}$$

Corrections proportional to ξ, especially in the prefactor of the logarithm in (87), can be important at moderately small $\Sigma_1^{-2}+\Sigma_2^{-2}$. Neglecting Ω^2 or ξ^2 under the logarithm sign in (87), we arrive correspondingly at Eq. (2.42) or (2.43) of [16]. In Fig. 7 we compare the behavior of function (86) (solid curve) with that of approximation (87) (dotted curve) and of an approximation resulting once we put in Eq. (86) $\xi\to 0$ (dashed curve). The latter two approximations are seen to work in complementary regions.

3. Asymmetric case

Finally, we examine the case when one of the foils scatters weakly, whereas another one scatters electrons through angles $\gg\gamma^{-1}$. Inserting the corresponding limiting forms (63b) and (64) into (57), we arrive at

$$\left\langle\frac{dI}{d\omega}\right\rangle\underset{\substack{\Sigma_1\ll 1\\ \Sigma_2\gg 1}}{\simeq}\frac{2e^2}{\pi c}\left\{\ln\Sigma_2^2-\gamma_{\rm E}-1+\frac{\Sigma_1^2}{3}[1+g_{\rm ql}(\Omega)]\right\}, \tag{88}$$

where

$$g_{\rm ql}(\Omega)=-6\int_0^\infty\frac{d\Theta^2\Theta^2}{(1+\Theta^2)^4}\cos\Omega(1+\Theta^2), \tag{89}$$

with $g_{\rm ql}(0)=-1$. Function (89) has a maximum at $\Omega\approx 1.6$.

Notably, there is no logarithmic dependence in the interference term, and its amplitude does not depend on Σ_2, which corresponds to strict saturation of the radiation. Correspondingly, the visibility in this case is $\sim\frac{\Sigma_1^2}{\ln\Sigma_2^2}$, i.e., even lower than for the case of double small-angle scattering.

VI. ACCOUNT FOR FOIL THICKNESS(ES)

Hitherto we presumed geometric thicknesses of both targets to be negligible, but at a sufficiently large ω, finite target thickness must inevitably manifest itself. Obviously, when l_f decreases down to the value of l, the target geometry gets resolved, and then the radiation spectrum must rise (from the doubled but logarithmically saturated values) to the completely saturation-free Bethe-Heitler plateau.

In principle, our framework requires only minor modification to reflect the mentioned rise: The radiation spectrum computed above must be multiplied by a plate form factor, which smoothly interpolates between unity at $\omega\lesssim\frac{2\gamma^2}{t_{21}}$ and Migdal's function Φ_M at $\omega\gg\frac{2\gamma^2}{t_{21}}$ (specifically, at $\frac{\omega}{c}\gtrsim\gamma^2\frac{l_{\rm scat}}{l^2}$, where $l_{\rm scat}\sim\alpha X_0$ is the length at which the electron scatters through angles $\sim\gamma^{-1}$). The implementation of such an interpolation, however, is beyond the scope of this paper.

VII. COMPARISON WITH EXPERIMENT

To accomplish our study, let us confront the predictions of our equations with experimental data. Measurements of bremsstrahlung spectra from 178 GeV electrons on a sequence of plates were performed in [18,19] with two equal 26 μm thick golden foils ($X_0^{\rm Au}=3.4$ mm) separated by a gap of variable width. The scattering strength parameter for one such a foil, according to Eq. (45), equaled $\gamma\sigma\approx 2.7$, so the scattering angles were substantial.

In Fig. 8 we compare predictions of our Eq. (57) and Eq. (71) with the experiment [19], letting ct_{21} be equal to the distance $l_{\rm g}+l$ between plate centers, where $l_{\rm g}$ is the gap width, and l are the thicknesses of each of the targets. The agreement may be regarded as fair. Experimental inaccuracies discussed in Ref. [18] may cause some systematic deviations at $\hbar\omega\lesssim 50$ MeV, but they seem to be commensurable with statistical uncertainties.

[9]However, we disagree with their interpretation of it as a unit-wavelength resonance. As was argued above, it is more appropriate to regard it as an inclined half-wavelength resonance. Besides that, Baier and Katkov conducted their evaluation of the maximum for a specific value of the target thickness 11 μm.

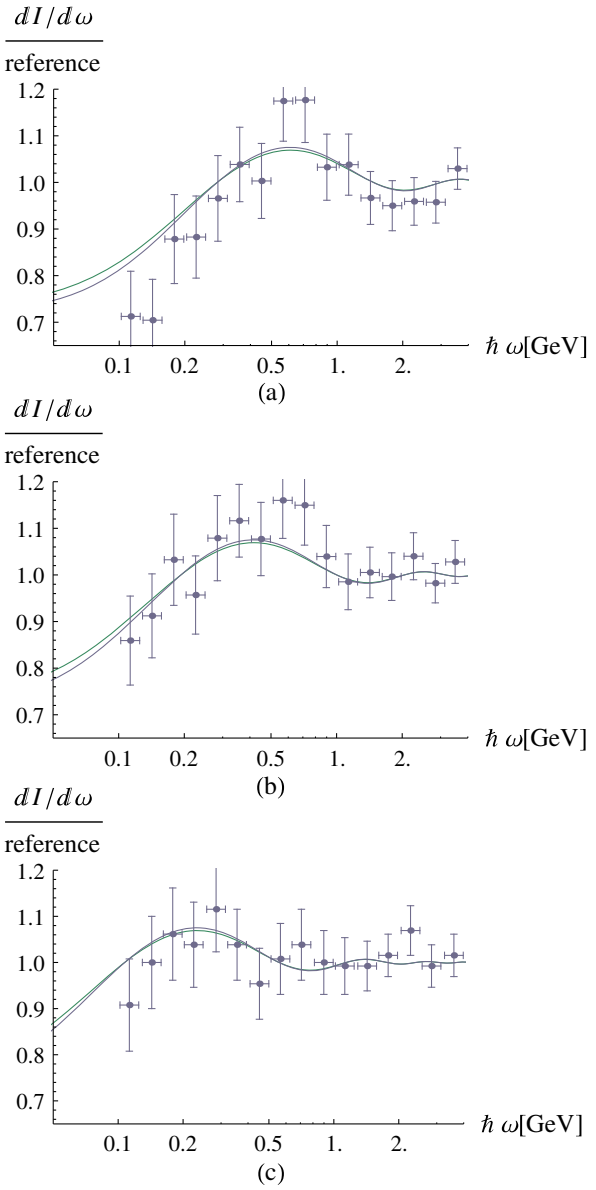

FIG. 8 (color online). Shapes of spectral oscillations for conditions of experiment [19] ($l_1 = l_2 = 26$ μm). (a) $ct_{21} = 26 + 60$ μm; (b) $ct_{21} = 26 + 100$ μm; (c) $ct_{21} = 26 + 200$ μm. Dark blue curves, Gaussian averaging, with Σ calculated by Eq. (45). Green curves, Molière averaging for gold.

Since our Gaussian and Molière averaging procedures give numerically close results (for the present experimental conditions), and on the other hand, it was found in Sec. III C that the Gaussian averaging procedure is equivalent to that of Baier and Katkov, it is likely that Baier and Katkov's predictions for the radiation spectrum must generally agree with the experiment [19] as well, provided one utilizes a reasonable prescription for the scattering angle. However, it was found in [19] (Fig. 5) that the position of the principal spectral maximum as predicted by Baier and Katkov disagrees with the experiment. That discrepancy must be attributed in the first place to the inaccuracy of extraction in [16] of the location of the spectral maximum from generic equations (2.34), (2.36) (see our discussion in Sec. IV B). In principle, though, Eqs. (2.34), (2.36) of [16] appear to be correct and may be used provided one evaluates the encountered double integrals numerically.

As for comparison of experimental results with predictions of Blankenbecler, recalling our results of Sec. V, it should be noticed that the use of plates with scattering strength $\gamma\sigma \approx 2.7$ closely corresponds to the point of intersection of visibilities in the Blankenbecler-Drell approximation with the exact ones [see Figs. 4(b), 5(b)]. Therefore, Blankenbecler's predictions may agree with the experiment [19] rather nicely, as well. Overall agreement of experimental results with [14] (and disagreement with [15]) was actually reported in [19]. However, for foils several times thinner than those used in [19] (or made of a lighter material), we expect inaccuracy of Blankenbecler-Drell predictions to be greater. At the same time, for weaker scattering foils, the visibility of *secondary* spectral minima and maxima can yet increase by almost a factor of 2 [see Figs. 5(b), 5(c)].

VIII. SUMMARY

We have explored the physical mechanisms behind constructive and destructive interference for bremsstrahlung on a structured amorphous target. In this case, the existence of constructive interference may seem counterintuitive, as long as the Bethe-Heitler spectrum of radiation at uncorrelated scatterings is ω-independent, whereas in the LPM spectrum taking account of nondipole effects the interference is purely suppressive. Nonetheless, enhancement in a certain spectral region for a structured amorphous target with substantial separation between the scattering foils is predicted by calculations and confirmed experimentally. Albeit the effect is not large (typically $\sim$10%) because of substantial cancellations of interference contributions to radiation in an amorphous medium, it is of fundamental significance. The main conclusions reached in the present study may be summarized as follows:

(i) The enhancement in the spectrum of bremsstrahlung on two foils occurs in the region next to the region of spectral suppression at lowest ω. The ω-integrated effect of suppression and enhancement is zero (see the end of Sec. II). The principal peak may be interpreted geometrically as an inclined-half-wavelength resonance [see Eq. (60)], but not as a unit-wavelength resonance, as was suggested previously [14].

(ii) The shape of the interference pattern, particularly the location of the principal maximum, has a noticeable dependence on the strength of multiple scattering in each plate (see Fig. 3). It assumes universal forms for limiting cases of strong or weak scattering: For small (compared to γ^{-1}) scattering angles in both

plates, the shape of the oscillatory pattern in the spectrum is described by Eq. (84). For large scattering angles in both plates, it is described by function (86) (unifying different limiting cases described in [16]). For the mixed case when one plate scatters weakly, while another one does so strongly, the spectrum shape obeys Eq. (88), where the dependence of the interference term on Σ_2 strictly saturates.

(iii) At asymptotically large ω, the dominant contribution to the interference term stems from photon emission directions close to the electron velocity $\boldsymbol{v}_2$ between the foils, such that $|\boldsymbol{n}-\boldsymbol{v}_2/c| < \sqrt{\frac{2}{\omega t_{21}}} < \frac{1}{\gamma}$. Therewith, the interference term scales as $\propto \frac{\cos\Omega}{\Omega^2}$, with the coefficient proportional to the product of G-amplitudes of radiation emitted strictly parallel to $\boldsymbol{v}_2$ [see Eq. (58)]. Granted this universality, the locations of *secondary* maxima and minima are basically independent of scattering strengths in the plates.

To aid experiment planning, we have expressed our results in terms of visibilities of the interference minima and maxima at low and at large ω depending on the target thicknesses (Sec. V, Figs. 4 and 5). In the meantime, predictions of classical electrodynamics are in agreement with the available experiment [19], for any averaging procedure (Gaussian, Molière, or Blankenbecler-Drell). However, for different target thicknesses the sensitivity to the averaging procedure can be greater.

For future theoretical applications, it may be noted that enhancing effect in bremsstrahlung spectra might manifest itself not only for artificial assemblies of plates, but also in continuous media (where it must be regarded as an anti-LPM effect), provided one finds a case when every constituent of the matter scatters the radiating projectile relativistically. The corresponding conditions, perhaps, may be fulfilled for passage of an ultrarelativistic quark through nuclear matter.

ACKNOWLEDGMENTS

The authors are indebted to U. I. Uggerhøj for providing us with the experimental data, and useful communications. This work was supported in part by the State Fund for Fundamental Research of Ukraine (Project No. F58/17).

APPENDIX: DERIVATION OF FORMULA (45) FROM MOLIÈRE DISTRIBUTION

The success of the Gaussian approximation for the angular distribution of multiple Coulomb scattering in conjunction with interpolation (45) for the rms scattering angle may be explained by examining the large-χ_c limit for the *radiation* form factor, formula (39):

$$\langle F\rangle_{\rm M} = 2\int_0^{\rho_0}\frac{d\rho}{\rho}\left\{1-e^{-\frac{1}{2}\rho^2\gamma^2\chi_c^2(\ln\frac{2}{\gamma\chi_1\rho}+\frac{1}{2}-\gamma_{\rm E})}\right\} + 2\int_{\rho_0}^{\infty}d\rho\rho K_1^2(\rho), \tag{A1}$$

where $\frac{2}{\gamma\chi_f} \ll \rho_0 \ll 1$. The second integral with the next-to-leading logarithmic accuracy equals

$$\int_{\rho_0}^{\infty}d\rho\rho K_1^2(\rho) = \ln\frac{2}{\rho_0}-\frac{1}{2}-\gamma_{\rm E},$$

whereas in the first integral one can approximately replace ρ^{-2} under the logarithm sign by its typical value $\rho^{-2}\sim\frac{\gamma^2\chi_c^2}{4}\ln\frac{\chi_c^2}{\chi_1^2}$, and compute the integral analytically, too:

$$\int_0^{\rho_0^2}\frac{d\rho^2}{\rho^2}\left\{1-e^{-\frac{1}{4}\rho^2\gamma^2\chi_c^2[\ln(\frac{\chi_c^2}{\chi_1^2}\ln\frac{\chi_c^2}{\chi_1^2})+1-2\gamma_{\rm E}]}\right\} = \ln\left\{\gamma^2\chi_c^2\left[\ln\left(\frac{\chi_c^2}{\chi_1^2}\ln\frac{\chi_c^2}{\chi_1^2}\right)+1-2\gamma_{\rm E}\right]\right\} - 2\ln\frac{2}{\rho_0}+\gamma_{\rm E}.$$

Combining the integrals and comparing the result with Eq. (23), we find an unambiguous relation for the effective mean square scattering angle

$$\Sigma^2 = \gamma^2\chi_c^2\left[\ln\left(\frac{\chi_c^2}{\chi_1^2}\ln\frac{\chi_c^2}{\chi_1^2}\right)+1-2\gamma_{\rm E}\right]. \tag{A2}$$

It differs from the corresponding estimate in the Bethe-Molière scattering theory by the term $1-2\gamma_{\rm E}=-0.15$, which, however, is relatively small and can safely be neglected.

To further express Σ^2 in terms of the radiation length, substitute $\frac{\chi_c^2}{\chi_1^2}$ from Eq. (44):

$$\Sigma^2 = \frac{\pi}{\alpha(\ln\frac{1}{\gamma^2\chi_1^2}+\frac{7}{6})}\frac{2l}{X_0} \times\left[\ln\frac{1}{\gamma^2\chi_1^2}+\ln\frac{\pi}{\alpha}+\ln\frac{\ln\frac{\chi_c^2}{\chi_1^2}}{\ln\frac{1}{\gamma\chi_1}+\frac{7}{12}}+\ln\frac{l}{X_0}\right]. \tag{A3}$$

Estimates of different contributions give $\ln\frac{\pi}{\alpha}\approx 6$, $\ln\frac{1}{\gamma^2\chi_1^2}\approx 8\pm 2$, $\ln\frac{\ln\frac{\chi_c^2}{\chi_1^2}}{\ln\frac{1}{\gamma\chi_1}+\frac{7}{12}}\sim 1$, whereas $\ln\frac{l}{X_0}$ varies from -7 (if $l=10^{-3}X_0$) to -2 (if $l=10^{-1}X_0$). Replacing all the terms except the last on by their average values leads to the result

$$\Sigma\approx\frac{\mu}{m_e}\sqrt{\frac{2l}{X_0}}\sqrt{1+2\epsilon\ln\frac{l}{X_0}}\approx\frac{\mu}{m_e}\sqrt{\frac{2l}{X_0}}\left(1+\epsilon\ln\frac{l}{X_0}\right), \tag{A4}$$

with $\mu\approx\sqrt{\frac{\pi}{\alpha}\frac{8+6+1}{8+7/6}}m_ec^2 = 13.6$ MeV, and $\epsilon\approx\frac{1}{2(8+6+1)} = 0.033$. Those numbers comply with the coefficients in

Eq. (45), which can therefore be regarded as inferred *ab initio*. Parameter μ may also be compared with Rossi's $E_s = \sqrt{\frac{4\pi}{\alpha}} m_e c^2 = 21.2$ MeV. Product $\mu(1 + \epsilon \ln \frac{l}{X_0})$ becomes twice smaller than E_s at $l \sim 10^{-3} X_0$, which then exactly corresponds to approximation (27). In general, of course, it is more accurate to use a formula with an explicit $\ln l/X_0$ dependence, like Eq. (45). A better approximation still would be to take into account also the Z-dependence, and Eq. (A3) suggests how to do that through the term $\ln \frac{1}{\gamma^2 \chi_1^2}$ in the numerator and denominator.

[1] M. L. Ter-Mikayelyan, *High Energy Electromagnetic Processes in Condensed Media* (Wiley, New York, 1972); V. N. Baier, V. M. Katkov, and V. S. Fadin, *Radiation from Relativistic Electrons* (in Russian) (Atomizdat, Moscow, 1973); A. I. Akhiezer and N. F. Shul'ga, *High Energy Electrodynamics in Matter* (Gordon & Breach, Amsterdam, 1996).

[2] L. D. Landau and I. Ya. Pomeranchuk, Dokl. Akad. Nauk SSSR **92**, 535 (1953); **92**, 735 (1953).

[3] A. B. Migdal, Phys. Rev. **103**, 1811 (1956).

[4] F. F. Ternovskii, Zh. Eksp. Teor. Fiz. **39**, 171 (1960) [Sov. Phys. JETP **12**, 123 (1961)].

[5] V. E. Pafomov, Zh. Eksp. Teor. Fiz. **49**, 1222 (1965) [Sov. Phys. JETP **22**, 848 (1966)].

[6] R. Blankenbecler and S. D. Drell, Phys. Rev. D **53**, 6265 (1996).

[7] B. G. Zakharov, Pis'ma Zh. Eksp. Teor. Fiz. **64**, 737 (1996) [JETP Lett. **64**, 781 (1996)]; Yad. Fiz. **61**, 924 (1998) [Phys. At. Nucl. **62**, 1008 (1998)].

[8] V. N. Baier and V. M. Katkov, Phys. Rev. D **57**, 3146 (1998).

[9] N. F. Shul'ga and S. P. Fomin, Pis'ma Zh. Eksp. Teor. Fiz. **27**, 126 (1978) [JETP Lett. **27**, 117 (1978)]; Zh. Eksp. Teor. Fiz. **113**, 58 (1998) [JETP **86**, 32 (1998)]; Nucl. Instrum. Methods Phys. Res., Sect. B **145**, 73 (1998).

[10] P. Anthony *et al.*, Phys. Rev. D **56**, 1373 (1997); H. D. Hansen, U. I. Uggerhøj, C. Biino, S. Ballestrero, A. Mangiarotti, P. Sona, T. J. Ketel, and Z. Z. Vilakazi, Phys. Rev. D **69**, 032001 (2004).

[11] S. Klein, Rev. Mod. Phys. **71**, 1501 (1999).

[12] A. I. Akhiezer, N. F. Shul'ga, and S. P. Fomin, *Landau-Pomeranchuk-Migdal Effect* (Cambridge Scientific Publishers, Cambridge, 2005).

[13] V. N. Baier and V. M. Katkov, Phys. Rep. **409**, 261 (2005).

[14] R. Blankenbecler, Phys. Rev. D **55**, 190 (1997); Stanford Report No. SLAC-PUB-96-7156, 1996.

[15] R. Blankenbecler, Phys. Rev. D **55**, 2441 (1997).

[16] V. N. Baier and V. M. Katkov, Phys. Rev. D **60**, 076001 (1999).

[17] H. D. Thomsen *et al.*, Phys. Rev. D **81**, 052003 (2010).

[18] K. K. Andersen, S. L. Andersen, J. Esberg, H. Knudsen, R. Mikkelsen, U. I. Uggerhøj, P. Sona, A. Mangiarotti, T. J. Ketel, and S. Ballestrero, Phys. Rev. Lett. **108**, 071802 (2012).

[19] K. K. Andersen *et al.*, Phys. Lett. B **732**, 309 (2014).

[20] G. Diambrini Palazzi, Rev. Mod. Phys. **40**, 611 (1968).

[21] J. D. Jackson, *Classical Electrodynamics*, 3rd ed. (Wiley, New York, 1998); L. D. Landau and E. M. Lifshitz, *The Classical Theory of Fields* (Elsevier, Oxford, 1975).

[22] J. S. Bell, Nucl. Phys. **B8**, 613 (1958).

[23] V. B. Berestetskii, E. M. Lifshitz, and L. P. Pitaevskii, *Quantum Electrodynamics* (Pergamon-Press, Oxford, 1982).

[24] B. Rossi, *High Energy Particles* (Prentice-Hall, New York, 1952).

[25] G. Moliere, Z. Naturforsch. **2A**, 133 (1947); **3A**, 78 (1948); H. A. Bethe, Phys. Rev. **89**, 1256 (1953).

[26] J. D. Bjorken, J. B. Kogut, and D. E. Soper, Phys. Rev. D **3**, 1382 (1971).

[27] R. J. Glauber, Phys. Rev. **100**, 242 (1955).

[28] Y.-S. Tsai, Rev. Mod. Phys. **46**, 815 (1974).

[29] U. Fano, Phys. Rev. **93**, 117 (1954).

[30] J. Beringer *et al.* (Particle Data Group), Phys. Rev. D **86**, 010001 (2012).

[31] V. L. Highland, Nucl. Instrum. Methods **129**, 497 (1975).

[32] G. R. Lynch and O. I. Dahl, Nucl. Instrum. Methods Phys. Res., Sect. B **58**, 6 (1991).

[33] M. Abramowitz and I. A. Stegun, *Handbook of Mathematical Functions* (Dover, New York, 1972).

[34] V. M. Galitsky and I. I. Gurevich, Nuovo Cimento **32**, 396 (1964).